Regge poles and elementary particles

R J EDEN

Cavendish Laboratory, University of Cambridge

Contents

Rep. Prog. Phys. 1971 **34** 995–1053

Abstract. This is a review of Regge theory that is intended both as an introduction to its main features and as a survey of its relation to experimental results on the strong interactions of elementary particles. It includes a survey of the experimental and theoretical background that is required for an understanding of Regge theory. The central part of the review describes the basic ideas of Regge theory and the application of Regge pole models to high-energy collisions of elementary particles. The review concludes with a brief account of extensions of Regge theory that give the Veneziano representation and that give some features of many-particle production in high-energy collisions.

1. Introduction

1.1. *Preliminary remarks*

Regge theory is concerned with the classification of elementary particles and resonances, and with the collisions of elementary particles at high energies. In its most general form it is not a predictive theory but it provides an important framework which gives a basis for a systematic study of the strong interactions of elementary particles. Within this framework Regge models can be constructed and tested by their predictions about high-energy reactions.

The objectives of this review are to give an introduction to Regge theory and to describe its relation to experimental results. The plan of the review commences with some definitions and introduces some of the language of high-energy physics. Next follows a survey of experimental results so as to illustrate what Regge theory is trying to explain. A brief account of some basic theoretical ideas is then followed by a section describing the main features of Regge theory and a section describing some of its applications and their relation to experiment. The final section of this review indicates some extensions from Regge theory which include a discussion of the idea of duality and the Veneziano representation.

In order to introduce the concepts and language of Regge theory as simply as possible I will concentrate mainly on the particular models in the theory that are based on Regge poles. A Regge pole is a singularity of the form $1/(J-\alpha)$ in a suitably chosen scattering amplitude, where J denotes angular momentum and α is a function of the energy of the colliding particles. This will be explained more precisely in §§ 3 and 4 of this article.

Regge models are phenomenological in character; they are developed and modified under the stimulus of experimental results. Section 2 of this review will therefore consist of a survey of some of the characteristic features of experiments on collisions that Regge models seek to explain or correlate or predict. Section 3 will contain a survey of the main features of relativistic collision theory or S matrix theory that form an essential background to the development of Regge models.

Regge theory is based on the use of complex angular momentum combined with relativistic collision theory. Originally, Regge (1959, 1960) developed the use of complex angular momentum to study nonrelativistic scattering by a Yukawa potential. The subsequent extension of Regge theory to give models for a relativistic

theory of collisions of strongly interacting elementary particles was initially due to Blankenbecler and Goldberger (1962), Chew and Frautschi (1961, 1962) and Gribov (1962a,b).

The use of complex angular momentum will be introduced in § 4 where we will describe the basic ideas of Regge theory. Further aspects of the theory will be developed in § 5, which is primarily concerned with illustrating the ways in which it can be compared with experimental results. Since the main objectives in this review are to describe the concepts and ideas of Regge theory rather than the technical details, we will avoid the complications due to the fermion spin formalism as far as possible. The reader who requires more technical details will find many of them discussed in an extensive review of Regge theory by Collins (1971).

References will be given in the text both to review articles and to original papers, but no attempt has been made to include all important original papers on Regge theory. Many of these are listed by Svensson (1967 unpublished), Collins and Squires (1968), Collins (1971) and Jackson (1969). The reader who seeks a wider introduction to the strong interactions of elementary particles than is given in this review may refer to elementary accounts given by Chew *et al* (1964) and Eden (1970), or to the more advanced accounts in the books by Martin and Spearman (1970), Pilkuhn (1968), Eden (1967) or Barger and Cline (1969).

1.2. *Units*

The conventional units in high energy physics take

$$\hbar = c = 1 \tag{1.1}$$

where $\hbar$ denotes Planck's constant h divided by 2π, and c denotes the velocity of light.

Energy and mass are measured in MeV or GeV, but momentum is often expressed in units of MeV/c, purely to distinguish it from an energy.

Cross sections are measured in millibarns,

$$1 \text{ mb} = 10^{-31} \text{ m}^2 = 0{\cdot}1 \text{ fm}^2 \tag{1.2}$$

where one femtometre (10^{-15} m) is commonly known as a fermi.

The pion mass is written μ or m_π, and the nucleon mass (neutron or proton) M (or m_n, m_p; $m_n \simeq m_p$). Their approximate values are

$$\mu \simeq 140 \text{ MeV} \qquad M \simeq 940 \text{ MeV}. \tag{1.3}$$

Conversion factors can be worked out using

$$\hbar = 6{\cdot}582 \times 10^{-22} \text{ MeV s} \qquad c \simeq 3 \times 10^8 \text{ m s}^{-1}. \tag{1.4}$$

This gives, for example,

$$1 \text{ GeV} \simeq 5 \text{ fm}^{-1} \qquad 1 \text{ GeV}^{-1} \simeq 0{\cdot}2 \text{ fm} \tag{1.5}$$

$$1 \text{ GeV}^{-2} \simeq 0{\cdot}389 \text{ mb} \simeq 0{\cdot}4 \text{ mb} \tag{1.6}$$

$$1 \text{ MeV}^{-1} \simeq 7 \times 10^{-22} \text{ s}. \tag{1.7}$$

The pion mass μ satisfies $50\mu^2 \simeq 1$ GeV^2 and

$$\mu^{-1} \simeq \sqrt{2} \text{ fm} \qquad \mu^{-2} \simeq 50 \text{ GeV}^{-2} \simeq 40 \text{ mb}. \tag{1.8}$$

1.3. *Quantum numbers*

Certain quantities are conserved absolutely in interactions of elementary particles, for example total energy and momentum, and total charge. Other quantities are almost conserved, thus total strangeness is conserved in strong interactions (which are our main concern in this review) and electromagnetic interactions, but total strangeness is not conserved in weak interactions.

The properties of elementary particles are described in an elementary manner in several textbooks or reviews and they will not be discussed here in any detail (see Chew *et al* 1964, Eden 1970, or the textbooks listed at the end of § 1.1). However, it may be useful to list briefly some of the most important properties and some (nearly) conserved quantities that can be used to label particles. These include:

(i) *Rest mass*: usually measured in MeV or GeV.

(ii) *Lifetime*: for example protons and electrons are stable, the π^+, π^- mesons have a half-life of order 10^{-8} s, the π^0 about 10^{-16} s. Resonances such as the $\Delta(1236)$, which is a resonance in a pion–nucleon collision, have a much shorter lifetime of order 10^{-23} s.

(iii) *Baryon number*: mesons have baryon number $B = 0$; protons, neutrons and hyperons have $B = 1$, antiprotons, etc have $B = -1$. Total baryon number is absolutely conserved.

(iv) *Charge Q*: charges on observed elementary particles and resonances range from $-e$ to $+2e$, where $-e$ is the charge on an electron. Total charge is absolutely conserved.

(v) *Spin J*: a fermion (eg proton or neutron) has half-odd-integer spin (in units of $h/2\pi$), a boson has integer or zero spin (eg pions have $J = 0$, the ρ meson has $J = 1$). The $\Delta(1236)$ resonance has spin $\frac{3}{2}$.

(vi) *Isospin I*: this is a vector operator, algebraically analogous to angular momentum. Its third component I_3 is related to charge, for example in the case of neutron or proton

$$Q = (I_3 + \tfrac{1}{2}).$$

(vii) *Strangeness S*: a strangeness quantum number is associated with each particle; π mesons and nucleons have $S = 0$, whereas Λ and Σ baryons have $S = -1$, and K^+ mesons have $S = +1$ but K^- mesons have $S = -1$. With the rule of strangeness conservation, one sees that the reaction

$$\pi^- + p \rightarrow \Sigma^- + K^+$$

has total $S = 0$ on both sides so it is an allowed reaction. However, the reaction

$$\pi^- + p \rightarrow \Sigma^+ + K^-$$

is not allowed since it has total $S = 0$ on the left-hand side but total $S = -2$ on the right-hand side.

(viii) *Parity P*: the absorption of a π meson by a deuteron causes a change in the reflection character of the space wavefunction from even to odd. One deduces that the pion has odd (or negative) parity. Parity is conserved in strong and electromagnetic interactions.

1.4. *Two-body reactions*

In this review we will be primarily concerned with two-body reactions. The relative simplicity of two-body systems permits more precision in the comparison

of Regge models with experiment than is feasible for multiparticle production, although Regge models can also be developed for the latter processes. Examples of two-body reactions are

$\pi^- p \to \pi^- p$ elastic scattering

$\pi^- p \to \pi^0 n$ charge exchange scattering

$\pi^- p \to K^0 \Lambda^0$ associated production (a strangeness exchange and charge exchange reaction).

In the second reaction (pion–nucleon charge exchange), the π^0 is not observed directly but may be observed from its decay

$$\pi^0 \to 2\gamma$$

with the photons observed, for example, by e^+e^- pair production. A similar situation occurs in the third reaction.

The following reactions are often called quasi-two-body reactions, since one or both of the final particles decays by strong interactions to the particles that are actually observed,

$$\pi^- p \to \rho^0(765)\, n \qquad (1.9)$$
$$\qquad\quad \hookrightarrow \pi^+\pi^-$$

$$\pi^- p \to \rho^0(765)\ \ \Delta^0(1236) \qquad (1.10)$$
$$\qquad\quad \hookrightarrow \pi^+\pi^- \hookrightarrow \pi^- p.$$

In reaction (1.9) the ρ^0 meson is distinguished by selecting those $\pi^+\pi^-$ pairs whose energy in their own centre of mass system (CM system), $E(\pi^+\pi^-)$, is near to 765 MeV. It is found that the production reaction

$$\pi^- p \to \pi^+\pi^- n \qquad (1.11)$$

has a resonance when $E(\pi^+\pi^-) = 765$ MeV whose width is about 125 MeV. This corresponds to a lifetime of order 5×10^{-24} s, which is comparable with the duration of the collision process. The nonresonant background of $\pi^-\pi^+$ production is not negligible but it can be subtracted from the observed results leaving results that correspond only to the quasi-two-body reaction (1.9). Similarly the reaction (1.10) producing the ρ^0 and Δ^0 resonances can be separated (approximately) from the production process in which the final particles are not in resonance states.

1.5. *Resonances and particles*

The $\Delta^0(1236)$ resonance observed in reaction (1.10) can also be observed as a resonance in $\pi^- p$ elastic scattering (see § 2). Its spin properties can be observed by studying the angular dependence of elastic scattering at the resonance energy of 1236 MeV in the CM system and it is found that $J = \frac{3}{2}$ and $l = 1$.

The spin properties of the ρ^0 meson can be determined by studying the angular distribution of the decay products $\pi^+\pi^-$ at an energy of 765 MeV in their CM system, and it is found that it has $J = 1$. It is found that a resonance also occurs in the $\pi^+\pi^0$ system and the $\pi^-\pi^0$ system at 765 MeV, but *not* in $\pi^+\pi^+$ or $\pi^-\pi^-$. It follows that the ρ meson has three charge states $(-, 0, +)$ so it has isospin 1.

A full list of observed particles and resonances is published periodically by particle data groups (see, for example, Barash-Schmidt *et al* 1971). In this review

it will be assumed that the reader is aware of the nearly stable particles, particularly pions (π^+, π^0, π^-), kaons ($K^-, K^0, \bar{K}^0, K^+$), $\eta^0(550)$, nucleons (n, p), hyperons ($\Lambda^0, \Sigma^-, \Sigma^0, \Sigma^+, \Xi^0, \Xi^-, \Omega^-$). However, when their properties are particularly relevant to the discussion, these will be stated in the context. The same will be done for the

Table 1. Particles and resonances (masses in MeV) taken from Barash-Schmidt *et al* (1971)

(*a*) *Stable or nearly stable particles*

$\gamma(0)$	$\nu_e, \nu_\mu(0)$	e(0·5) $\mu(105)$
$\pi^{\pm}(140)$	p(938·3)	
$\pi^0(135)$	n(939·6)	$\Xi^0(1315)$
$K^{\pm}(494)$	$\Lambda(1116)$	$\Xi^-(1321)$
$K^0(498)$	$\Sigma^+(1189)$	$\Omega^-(1672)$
$\eta(549)$	$\Sigma^0(1193)$	
	$\Sigma^-(1197)$	

(*b*) *Mesons and meson resonances*

$\pi(140)$	$\varphi(1019)$	$\varphi_N(1650)$
K(494)	$\eta_0^+(1070)$	$\rho_N(1660)$
$\eta(549)$	A1(1070)	$\rho(1710)$
		L(1770)
K(892)	B(1235)	S(1930)
η_0^+ (or ε) (700 to 1000)	f(1260)	U(2375)
$\rho(765)$	D(1285)	
$\omega(784)$	A2(1310)	
	K(1420)	
$\eta'(958)$	E(1422)	
$\delta(962)$	f′(1514)	
$\pi_N(975)$	$\pi/\rho(1540)$	
$\pi_N(1016)$	$\pi_A(1640)$	

(*c*) *Baryons and baryon resonances*

p(938·3)	$\Delta(1236)$	$\Lambda(1116)$	$\Sigma(1190)$
n(939·6)	$\Delta(1650)$	$\Lambda(1405)$	$\Sigma(1385)$
N′(1520)	$\Delta(1670)$	$\Lambda'(1520)$	$\Sigma(1670)$
N′(1535)	$\Delta(1890)$	$\Lambda'(1670)$	$\Sigma(1750)$
N(1670)	$\Delta(1910)$	$\Lambda''(1090)$	$\Sigma(1765)$
N(1688)	$\Delta(1950)$	$\Lambda(1815)$	$\Sigma(1950)$
N″(1700)	$\Delta(2420)$	$\Lambda(1830)$	$\Sigma(2030)$
N″(1780)	$\Delta(2850)$	$\Lambda(2100)$	$\Sigma(2250)$
N(1860)	$\Delta(3230)$	$\Lambda(2350)$	$\Sigma(2455)$
N(2190)	—	—	$\Sigma(2620)$
N(2220)	—	—	
N(2650)	$\Xi(1314)$	$\Omega^-(1672)$	
N(3030)	$\Xi(1530)$		
	$\Xi(1820)$		
	$\Xi(1940)$		

Antiparticles are not listed and it should be noted that many of the particles have several different charge states.

resonances that are used to illustrate experimental features or properties of Regge theory. In particular we will find the relation between the masses and angular momenta of certain sequences of resonances to be of special importance. A list of elementary particles and resonances that have been observed is shown in table 1.

Except for the nearly stable mesons, all the particles listed in table 1(*b*) have to be observed as resonances in final-state interactions in production processes as mentioned above in § 1.4. Many of the baryon resonances can also be observed in this way but most of those shown in table 1(*c*) have been confirmed by phase-shift analysis of two-body elastic scattering of pions or kaons by nucleons.

A review of the experimental and theoretical techniques in bubble chamber physics which have led to the discovery of many of these resonances is given by Kalmus (1972), who also outlines the basic properties of some of these resonances. We note here only that in table 1(*c*) p, n, N, N′, N″ and Δ have strangeness $S = 0$, whereas Λ, Λ′, Λ″ and the Σ sequence has $S = -1$, the Ξ sequence has $S = -2$, and for Ω^- the strangeness $S = -3$. These and other quantum numbers of particles will be noted in the context of our later discussion whenever they are of significance to the reasoning.

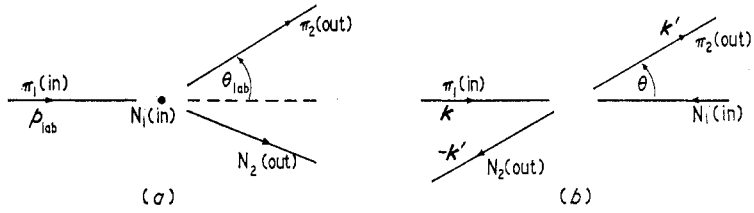

Figure 1. (*a*) Momenta in the laboratory system for a pion incident on a nucleon target. (*b*) Momenta in the CM system for a pion–nucleon collision.

1.6. *Kinematics for πN collisions*

Pion–nucleon kinematics will be required for illustrative purposes in the experimental survey of § 2. More detailed kinematics will be considered in § 3.

An energy–momentum four-vector will be denoted p (or p_0, $\boldsymbol{p}$) and we shall use the metric giving

$$p^2 = p_0{}^2 - \boldsymbol{p}^2. \tag{1.12}$$

Thus for a particle of mass m

$$p^2 = p_0{}^2 - \boldsymbol{p}^2 = m^2 \qquad p_0 = (m^2 + \boldsymbol{p}^2)^{1/2}. \tag{1.13}$$

We consider pion–nucleon elastic scattering

$$\pi_1 + \mathrm{N}_1 \to \pi_2 + \mathrm{N}_2. \tag{1.14}$$

The corresponding four-vectors will be written q_1, q_2 for the incoming and outgoing pions, and p_1, p_2 for the nucleons. Energy and momentum must be conserved so

$$q_1 + p_1 = q_2 + p_2. \tag{1.15}$$

The incoming and outgoing momenta are illustrated in figure 1(*a*) for the laboratory system in which the nucleon N_1 is at rest, and in figure 1(*b*) for the CM system.

In the πN CM system, conservation of energy gives $\boldsymbol{k}^2 = \boldsymbol{k}'^2$, where $\boldsymbol{k}, \boldsymbol{k}'$ denote the initial and final momenta in the CM system and the total energy W is

$$(\mu^2 + k^2)^{1/2} + (M^2 + k^2)^{1/2} = W = s^{1/2}. \tag{1.16}$$

This also defines the important variable s, which is the square of the total energy in the CM system.

The scattering angle θ in the CM system is related to the three-momenta $\boldsymbol{k}$ and $\boldsymbol{k}'$ by

$$\begin{aligned}\boldsymbol{k}.\boldsymbol{k}' &= |\boldsymbol{k}||\boldsymbol{k}'|\cos\theta \\ &= k^2\cos\theta. \end{aligned} \tag{1.17}$$

The momentum transfer from nucleon to pion in the collision in the CM system is $(\boldsymbol{k}'-\boldsymbol{k})$. The important variable t is defined to be minus the momentum transfer squared,

$$t = -(\boldsymbol{k}'-\boldsymbol{k})^2 = -2k^2(1-\cos\theta). \tag{1.18}$$

The importance of the variables s and t arises because they are relativistic invariants. For an arbitrary frame of coordinates, they are given in terms of the four-vectors by the equations,

$$s = (q_1+p_1)^2 = (q_2+p_2)^2 \tag{1.19a}$$

$$t = (q_1-q_2)^2 = (p_1-p_2)^2. \tag{1.19b}$$

Furthermore, if we neglect the spin of the nucleon, the whole result of the scattering process can be expressed in terms of s and t. That is to say, the scattering amplitude, F say, is a function of s and t only, $F(s,t)$. The same is true of the differential cross section.

Using (1.16) we see that

$$s = \{(M^2+k^2)^{1/2}+(\mu^2+k^2)^{1/2}\}^2$$

so the momentum $\boldsymbol{k}$ in the CM system satisfies

$$k^2 = \boldsymbol{k}^2 = \frac{(s-\mu^2-M^2)^2-4\mu^2M^2}{4s} \tag{1.20}$$

where we have used k to denote $|\boldsymbol{k}|$.

We can obtain the energy and momentum of the pion in the laboratory system by using the invariance of s and t. This gives

$$\begin{aligned} s &= M^2+\mu^2+2ME_\pi(\text{lab}) \\ &= M^2+\mu^2+2M(\mu^2+\boldsymbol{p}_{\text{lab}}^2)^{1/2}. \end{aligned} \tag{1.21}$$

At high energies this becomes

$$s \simeq 2M|\boldsymbol{p}_{\text{lab}}| \simeq 2|\boldsymbol{p}_{\text{lab}}| \quad (\text{GeV}^2) \tag{1.22}$$

since for a nucleon $M \simeq 1$ GeV.

1.7. *The physical scattering region*

For the pion–nucleon scattering illustrated in figures 1(*a*) and (*b*) to occur as an observable physical process, it is clearly necessary that the angles of scattering are real and the four-vectors are real Lorentz vectors that satisfy the appropriate mass shell condition analogous to equation (1.13). These conditions determine a region of the s,t plane (also called the 'Mandelstam plane') in which process (1.14) is physically allowed. This 'physical region' of the s,t plane can be found from equation (1.18) using $-1 \leqslant \cos\theta \leqslant 1$ and (1.20). Thus,

$$s \geqslant (M+\mu)^2 \tag{1.23}$$

and

$$-4k^2 \leqslant t \leqslant 0$$

or, using (1.20),

$$4\mu^2 M^2 - (s - \mu^2 - M^2)^2 \leqslant st \leqslant 0. \tag{1.24}$$

The physical region, whose boundaries are defined by equations (1.23) and (1.24), is illustrated in figure 2.

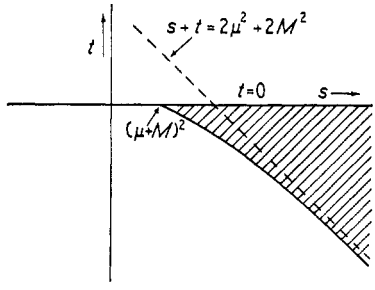

Figure 2. The physical region of the s, t plane for πN scattering.

1.8. *Cross sections and collision amplitudes*

Differential cross sections are measured in the laboratory system. The procedure is illustrated in figure 3(a) in which the counter records the number of pions elastically scattered into a solid angle $d\Omega$(lab) per unit time. The elastic differential cross section for scattering of pions on protons is defined by

$$\frac{d\sigma(\text{elastic})}{d\Omega(\text{lab})} = \frac{N(\text{out through counter})}{N(\text{incoming per proton})} \tag{1.25}$$

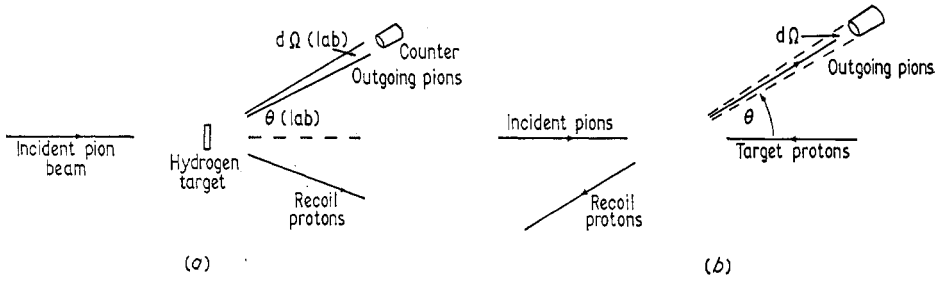

Figure 3. (a) Schematic diagram for defining a differential cross section in the laboratory system. (b) Scattering into solid angle $d\Omega$ in the CM system.

where the numerator denotes the number of elastically scattered pions per unit time crossing the area $r^2\,d\Omega$(lab) of the counter. The denominator on the right-hand side of (1.25) denotes the number of pions in the incident beam per unit area per unit time divided by the number of protons per unit area in the hydrogen target. The differential cross section (1.25) clearly has the dimensions of an area.

Using the kinematics discussed earlier in § 1.6, one can express the laboratory scattering angle θ(lab) via cos θ(lab) in terms of the invariants s and t. Then, using the relation $d\Omega(\text{lab}) = d\phi(\text{lab})\,d(\cos\theta(\text{lab}))$, one can express (1.25) in terms of $(d\sigma/dt)$ multiplied by certain kinematic factors.

The differential cross section in the pion–proton CM system can be similarly defined using the CM system scattering angle θ and the CM system azimuthal angle ϕ

(also equal to ϕ(lab)). The definition is illustrated in figure 3(b). We can write

$$d\Omega = d(\cos\theta)\, d\phi \tag{1.26}$$

and if we either ignore proton spin, or average over it, there will be no dependence of the differential cross section on ϕ. Hence

$$\int d\phi \frac{d\sigma}{d\Omega} = 2\pi \frac{d\sigma}{d\Omega} \equiv \frac{d\sigma(\text{elastic})}{d(\cos\theta)}. \tag{1.27}$$

From equation (1.18) we obtain

$$dt = 2k^2\, d(\cos\theta) \tag{1.28}$$

which gives

$$\frac{d\sigma(\text{elastic})}{dt} = \left(\frac{\pi}{k^2}\right) \frac{d\sigma(\text{elastic})}{d\Omega} \tag{1.29}$$

where the right-hand side is defined in the CM system. The left-hand side is an invariant and, as noted above, it may also be expressed in terms of the differential cross section (1.25) defined in the laboratory system.

If we neglect nucleon spin, the invariant differential cross section (1.29) may be expressed in terms of a single invariant scattering amplitude $F(s, t)$, where s and t are defined by (1.19a and b)

$$\frac{d\sigma(\text{elastic})}{dt} = \frac{1}{64\pi s k^2} |F(s, t)|^2. \tag{1.30}$$

This relation uses the conventional relativistic normalization for $F(s, t)$, but the reader should note that some authors choose different normalizations. If proton spin is taken into account there are two invariant scattering amplitudes for elastic pion–proton scattering.

If the differential cross section (1.30) is integrated over θ from 0 to π we obtain the integrated elastic cross section,

$$\sigma(\text{elastic}) = \int_{t_1(s)}^{0} dt \frac{d\sigma(\text{elastic})}{dt} \tag{1.31}$$

where t_1 denotes the lower limit for t at fixed s in equation (1.24) (see also figure 2).

Differential cross sections for two-body reactions

$$a + b \to c + d \tag{1.32}$$

are defined in a manner similar to that illustrated in figure 3(a) except that a second counter (or several counters) is required to identify the final particles c and d. The reaction differential cross section is given (neglecting possible spins of abcd) by

$$\frac{d\sigma(ab \to cd)}{dt} = K(s) |F_{abcd}(s, t)|^2 \tag{1.33}$$

where $K(s)$ denotes a kinematic factor. By integrating over physical values of t at fixed energy (fixed s), one obtains $\sigma(ab \to cd)$.

Total cross sections are equal to the sum of all allowed elastic and reaction cross sections including those involving many-body production,

$$\sigma_T(\pi^+ p) \equiv \sigma(\pi^+ p, \text{total}) = \sum \sigma(\pi^+ p \to \text{anything}). \tag{1.34}$$

In practice $\sigma_T(\pi^+ p)$ is obtained experimentally by measuring the number of particles removed from the incident pion beam. This is achieved by extrapolating to zero angle as illustrated in figure 4(*a*). The counters C_i subtend an angle Ω_i at the target. They detect the passage of charged particles. From the flux through these counters, and from the flux in the incident beam, one can obtain the number

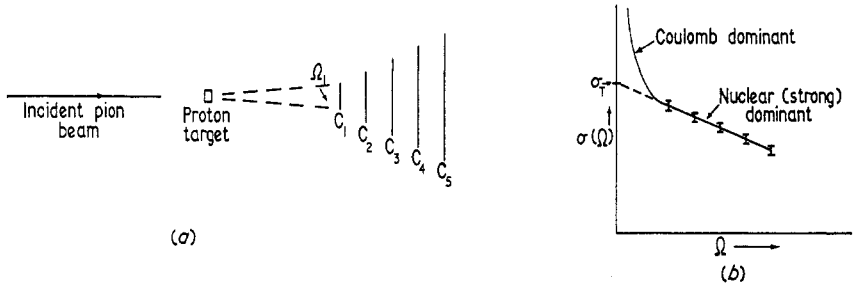

Figure 4. (*a*) Schematic diagram showing counters $C_1\,C_2\,C_3\,C_4\,C_5$ for measuring total cross sections. (*b*) Extrapolation to zero solid angle Ω to give a total cross section σ_T.

of particles removed from the incident beam by collision with the target. For each solid angle Ω_i one obtains (per unit time),

$$\sigma(\Omega_i) = \left(\frac{\text{no. of } \pi^+ \textit{ not} \text{ going into angle } \Omega_i}{\text{no. of } \pi^+ \text{ in incident beam per proton in target}}\right). \tag{1.35}$$

Extrapolating to $\Omega_i = 0$, but ignoring the coulomb dominant region, one obtains the total cross section as illustrated in figure 4(*b*),

$$\sigma_T(\pi^+ p, s) = \lim_{\Omega \to 0} \sigma(\Omega) \tag{1.36}$$

where s denotes the invariant energy variable.

Total cross sections are related to elastic scattering amplitudes by the optical theorem. This gives, for example,

$$\sigma_T(\pi^+ p) = \frac{\operatorname{Im} F(s, 0)}{2ks^{1/2}} \tag{1.37}$$

where $\operatorname{Im} F(s, 0)$ denotes the imaginary part of the $\pi^+ p$ forward elastic scattering amplitude. A detailed review of total cross sections has been given recently by Giacomelli (1970).

The central theoretical problem in collision processes is to find a method for evaluating the scattering amplitudes $F(s, t)$ and other collision amplitudes. We will see later in this review that Regge theory provides a framework within which attempts can be made via Regge models to calculate $F(s, t)$ and other amplitudes at high energies. However, we will proceed now with a description of the experiments that one is trying to explain.

2. Experimental survey

The principal types of experiments performed at high energies will be surveyed in this section. For the applicability of Regge models, high energies correspond to laboratory energies greater than about 5 GeV, but in some cases it is useful to consider energies below this limit. Observed resonances in two-body systems occur

below 5 GeV but we will not discuss the detailed evidence for these resonances, since it will be considered in the review by Kalmus (1972) in this series. We will, however, describe results of quasi-two-body reactions of the type discussed in § 1.4 in which resonances are regarded as particles in the final state.

In describing experimental data I will frequently make two simplifications to aid interpretation, the first being to avoid exhibiting all experimental points although typical experimental errors will be illustrated. The second simplification is the use of smooth curves drawn by eye through the experimental points; on occasions only these smooth curves will be given and the actual experimental points will be omitted.

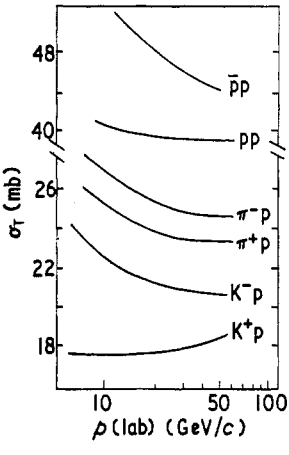

Figure 5. Total cross sections as a function of laboratory momentum from 5 to 65 GeV/c (from Denisov *et al* 1971).

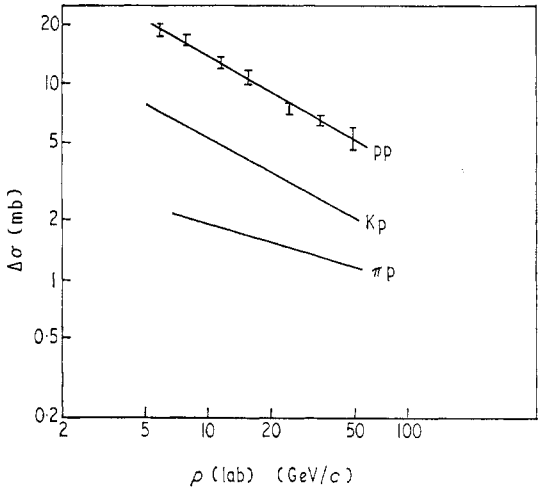

Figure 6. $\Delta\sigma = \sigma_T(\bar{a}, p) - \sigma_T(a, p)$, where $\bar{a}$, a denote $\bar{p}$, p or K^-, K^+ or π^-, π^+, respectively, plotted as a function of laboratory momentum (note that both scales are logarithmic) (from Denisov *et al* 1971).

2.1. *Total cross sections*

Total cross sections have been accurately measured for energies up to 70 GeV which is the highest available energy at the present time and is given by the proton accelerator at Serpukhov in the USSR. The data (Denisov *et al* 1971) for σ(total) for charged particles is shown in figure 5, for an energy range 5 to 70 GeV. The statistical errors for σ_T(pp) are $\pm 0{\cdot}25\%$, and the systematic scale errors are $\pm 0{\cdot}4\%$. For $\pi^{\pm}$p and K^+p the statistical errors are about $0{\cdot}5\%$ and the scale errors are similar. $\sigma_T(K^-p)$ and $\sigma_T(K^+p)$ are known with similar accuracy but $\sigma_T(\bar{p}p)$ has statistical errors around 1%.

The data shown in figure 5 indicate a smooth variation in σ_T for all processes above an energy of 5 GeV. Except for K^+p, where σ_T shows a slight increase between 15 and 55 GeV, all the cross sections appear to be decreasing, possibly towards an asymptotically constant value. The exceptional behaviour of $\sigma_T(K^+p)$ may be very significant in assessing the latter possibility.

It was originally suggested on intuitive grounds by Pomeranchuk (1956, 1958) that total cross sections should tend to constant values at high energies and also that particle–target and antiparticle–target total cross sections should become

asymptotically equal. The latter possibility is also given some support by the data in figure 5. It may be seen that $\sigma_T(\bar{p}p)$ decreases towards $\sigma_T(pp)$ as the energy increases. The convergence of particle–target and antiparticle–target total cross sections is also indicated by the results for $\pi^{\pm}p$ and for $K^{\pm}p$. The fact that $\sigma_T(\bar{p}p)$ is larger than $\sigma_T(pp)$ at lower energies may be qualitatively explained by the presence of a larger number of open channels for $\bar{p}p$, (annihilation giving meson final states for example) than for pp. At high energies these extra open channels for $\bar{p}p$ become relatively less important. It is also of interest to note that the $\bar{p}p$ system has many (mesonic) resonances observable at low energies whereas the pp system has none. Similar situations occur with π^-p and π^+p, and with K^-p and K^+p. The former in each case have more open channels than the latter, and they have more resonances than the latter.

The differences between particle and antiparticle total cross sections are shown in figure 6, where

$$\Delta\sigma(\pi p) = \sigma_T(\pi^- p) - \sigma_T(\pi^+ p) \tag{2.1}$$

and $\Delta\sigma(pp)$, $\Delta\sigma(Kp)$ have analogous definitions. The parametrization indicated by figure 6 takes the form (Denisov *et al* 1971)

$$\Delta\sigma = Ap^{-n} \tag{2.2}$$

where

$$A(pp) = 56{\cdot}8 \pm 5{\cdot}3 \text{ mb} \qquad n(pp) = 0{\cdot}61 \pm 0{\cdot}03$$

$$A(Kp) = 19{\cdot}2 \pm 1{\cdot}3 \text{ mb} \qquad n(Kp) = 0{\cdot}56 \pm 0{\cdot}02$$

$$A(\pi p) = 3{\cdot}88 \pm 0{\cdot}35 \text{ mb} \qquad n(\pi p) = 0{\cdot}31 \pm 0{\cdot}04.$$

The parametrization in equation (2.2) may be an oversimplification; Lindenbaum (1969) has noted that the data can be fitted in a way that is more consistent with dispersion relations for πp scattering by

$$\Delta\sigma(\pi p) \simeq 20p^{-0{\cdot}6} - 25p^{-1{\cdot}0}. \tag{2.3}$$

Then for large values of p, the graph for πp in figure 6 would become parallel to the other two graphs. The latter result can also be established on a fundamental theoretical basis (Roy 1972, see also § 2.5).

Cross sections involving neutrons have also been measured by collisions on a deuterium target. There is a little theoretical uncertainty in separating the contributions to σ_T from protons but in practice the Glauber method is expected to give a good approximation (Glauber 1955, Franco and Glauber 1966). The resulting total cross sections on neutrons are similar to those shown in figure 5, but with somewhat larger errors.

Experiments on total cross sections have recently been reviewed by Giacomelli (1970).

2.2. *Phases of forward amplitudes*

Using the optical theorem, measurements of σ_T give the imaginary part of the corresponding elastic forward amplitude, as shown in equation (1.37). The phase of $F(s, 0)$, and hence the real part $\mathrm{Re}\,F(s, 0)$, may be found from a coulomb interference experiment. This measures the differential cross section $d\sigma/dt$ in the region $t \sim -0{\cdot}002$ GeV^2 where the strong nuclear interactions are comparable with

coulomb effects.

$$\frac{d\sigma}{dt} = \frac{1}{64\pi s k^2}\left|-\frac{8\pi s^{1/2} G(t)}{|t|}\exp(2i\delta) + \mathrm{Re}\,F(s,t) + i\,\mathrm{Im}\,F(s,t)\right|^2 \tag{2.4}$$

where δ denotes the relative coulomb nuclear phase shift (Bethe 1958, West and Yennie 1968) and $G(t)$ is the product of the pion–nucleon form factors. Using measurements of $d\sigma/dt$ in the small t region, Foley *et al* (1967) obtain values for the ratio

$$\rho(s) = \frac{\mathrm{Re}\,F(s,0)}{\mathrm{Im}\,F(s,0)}. \tag{2.5}$$

Their results give at 20 GeV

$$\rho(\pi^- p) \simeq -0{\cdot}1 \qquad \rho(\pi^+ p) \simeq -0{\cdot}2.$$

Both are slowly increasing in the range 8 to 22 GeV, that is, $\mathrm{Re}\,F(s,0)$ appears to be tending towards zero. These results have been reviewed by Lindenbaum (1969).

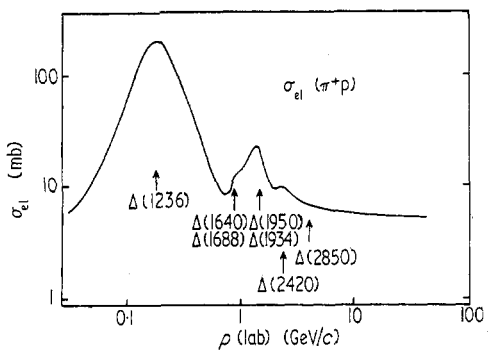

Figure 7. The integrated elastic cross section $\sigma_{el}(\pi^+ p)$ as a function of laboratory momentum, both scales are logarithmic (from Giacomelli 1971 unpublished).

2.3. *Elastic cross sections (integrated)*

The integrated elastic cross section $\sigma_{el}(\pi^+ p)$ is shown in figure 7. The locations of several resonances are shown on the drawing for $\sigma_{el}(\pi^+ p)$. Their existence cannot be deduced from bumps in σ_{el} alone but requires a phase-shift analysis (see § 3).

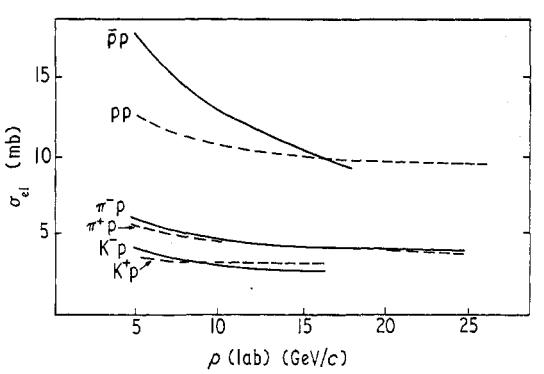

Figure 8. Integrated elastic cross sections as functions of laboratory momentum for $\bar{p}p$, pp, $\pi^- p$, $\pi^+ p$, $K^- p$ and $K^+ p$ scattering (from Giacomelli 1971).

At high energies, we see from figure 8 that σ_{el} becomes smooth both for $\pi^+ p$ and for $\pi^- p$. It is of interest to compare σ_{el} with σ_T. This is done in figure 9 which shows the ratio of σ_{el} to σ_T for p, $\bar{p}$, K^+, K^-, π^+, π^-, collisions on protons; it can be seen that the ratio $X = \sigma_{el}/\sigma_t$, satisfies

$$\left.\begin{aligned} X(\bar{p}p) &< X(pp) \\ X(\pi^- p) &< X(\pi^+ p) \\ X(K^- p) &< X(K^+ p). \end{aligned}\right\} \tag{2.6}$$

This result might have been expected because the left-hand pairs ($\bar{p}p$, etc) have

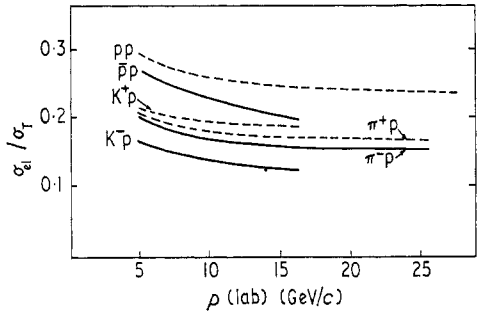

Figure 9. The ratio of σ_{el} to σ_T as a function of laboratory momentum for $\bar{p}p$, pp, $\pi^- p$, $\pi^+ p$, $K^- p$ and $K^+ p$ (from Giacomelli 1971).

more inelastic channels available than have those on the right-hand side. However, it is less expected that the difference $X(pp) - X(\bar{p}p)$ should increase as a function of the energy.

2.4. *Differential elastic cross sections*

A selection of the experimental results on elastic differential cross sections is shown on a logarithmic plot in figure 10. The strong forward peak is typical of diffraction scattering in which the behaviour at $t = 0$ is dominated by $\mathrm{Im}\,F(s, 0)$. Thus, using equations (1.30) and (1.37),

$$\left(\frac{d\sigma(\text{elastic})}{dt}\right)_{t=0} = \frac{(\sigma_T)^2}{16\pi} + \frac{(\mathrm{Re}\,F)^2}{64\pi s k^2}. \tag{2.7}$$

Thus if $\mathrm{Re}\,F(s, 0)$ is small compared with $\mathrm{Im}\,F$, both sides of (2.7) will be approximately constant as the energy s increases. Since the integrated elastic cross section is itself nearly constant, this demands a sharp peak in $d\sigma/dt$ at $t = 0$.

As we will see later, the simplest form of a Regge model indicates that for small t and large s,

$$\frac{d\sigma(\text{elastic})}{dt} \sim f(t) \left(\frac{s}{s_0}\right)^{2\alpha(t)-2}. \tag{2.8}$$

The 'effective' experimental value of $\alpha(t)$ has been evaluated by Fox and Quigg (1970), who compare (2.8) at fixed t with the s dependence of $d\sigma/dt$ given by the

experimental results from which the curves in figure 10 have been drawn. Their results are shown in figure 11.

The value of $\alpha(t)$ near $t = 0$ is less than 1, for $\pi^{\pm}$p and $\bar{p}$p scattering (possibly also K^-p). This reflects the fact that $\sigma_T(\pi^{\pm}p)$ and $\sigma_T(\bar{p}p)$ in equation (2.7) are decreasing functions of energy in the range 5 to 20 GeV from which figure 10 was

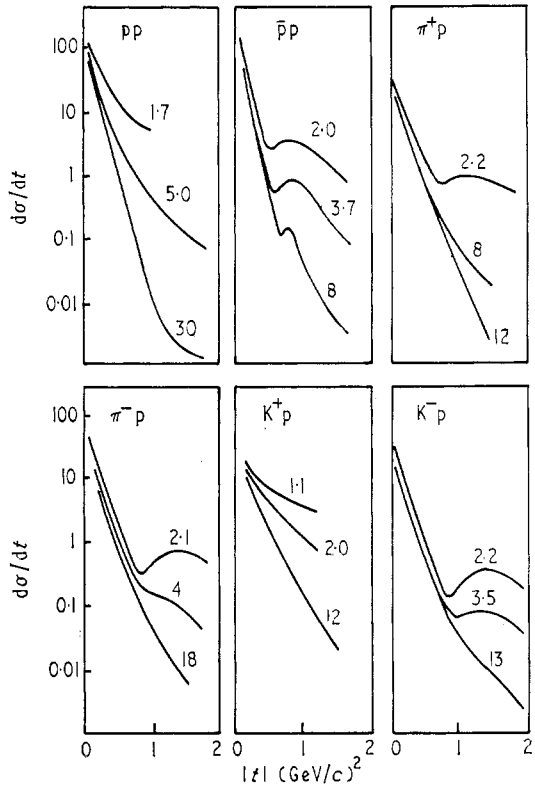

Figure 10. Differential cross sections measured in mb/(GeV/c)^2 for scattering on protons of p, $\bar{p}$, π^+, π^-, K^+, K^-, as functions of $|t|$ at various energies (from Allaby 1970).

obtained (see figure 5 for σ_T as a function of energy). For $\pi^{\pm}$p it has also been found that Re $F(s, 0)$ decreases but its square gives only a few per cent contribution to the right-hand side of equation (2.7) near $t = 0$. On the other hand, $\alpha(t)$ tends to 1 as t tends to zero for K^+p and for pp elastic scattering. This reflects the fact that σ_T is nearly constant for K^+p and pp collisions as was seen in figure 5.

Finally one should notice the dips in $d\sigma/dt$ shown in figure 10. The dip does not occur for pp or K^+p, but is present in the other four cases. However, its relative size decreases as the energy increases.

2.5. *Exchange cross sections*

The integrated charge-exchange cross section for the process

$$\pi^- p \to \pi^0 n \tag{2.9}$$

is shown in figure 12 on a log–log plot. Its linear form indicates that in the range

5 to 50 GeV/c

$$\sigma_{ex}(\pi^- p \to \pi^0 n) \simeq A(p(\text{lab}))^{-1\cdot17}. \tag{2.10}$$

It will be recalled that p(lab) is proportional to s at high energies.

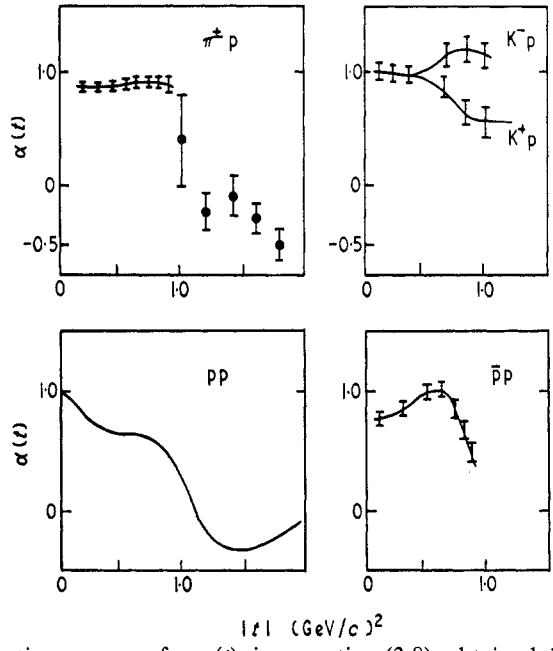

Figure 11. The effective power of s, $\alpha(t)$ in equation (2.8) obtained by comparison with experiments done at several different energies (Fox and Quigg 1970).

From the optical theorem and using isospin invariance $\text{Im}F_{ex}(s,0)/(2ks^{1/2})$ is proportional to $\Delta\sigma = \sigma_T(\pi^- p) - \sigma_T(\pi^+ p)$. Thus, if $\text{Im}F_{ex}$ and $\text{Re}F_{ex}$ were of similar magnitude at $t = 0$, one would expect the negative power 1·17 in equation (2.10) to be approximately twice that of $n(\pi p)$ in equation (2.2). Since $2n(\pi p) = 0{\cdot}62 \pm 0{\cdot}08$, there is rather a large discrepancy, which indicates that the parametrization in equations (2.2) and (2.10) is not very good.

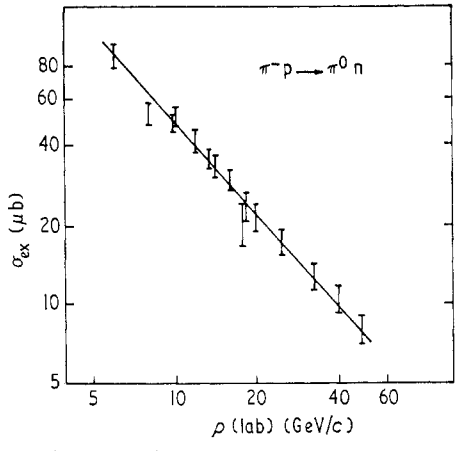

Figure 12. The integrated charge-exchange cross section for $\pi^- p \to \pi^0 n$ as a function of laboratory momentum (Giacomelli 1970).

Further evidence of complexity in the charge-exchange process is provided by the differential cross sections shown in figure 13. There is a dip in the forward direction, which shows that the spin effects due to the proton and neutron play a significant role. Indeed there must be a large spin-flip term (which vanishes at $t = 0$) in order to explain the forward dip.

The pronounced dip in $d\sigma_{ex}/dt$ seen in figure 13 at $|t| = 0{\cdot}6$ (GeV/c)^2 remains present up to the highest energies. This is in contrast with the dips in elastic scattering (figure 10) which disappear as the energy increases.

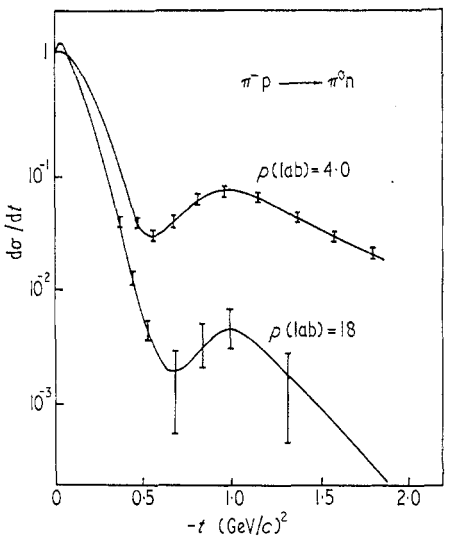

Figure 13. Normalized differential cross sections for $\pi^- p \to \pi^0 n$ (from Sonderegger *et al* 1966).

Another example of an exchange cross section of exceptional importance is given by K^0 regeneration, namely

$$K_L^0 + p \to K_S^0 + p. \tag{2.11}$$

In this reaction the long-lived component of K^0, which decays primarily into three pions, is converted by the interaction to the short-lived component that decays primarily into two pions. Using isospin invariance the amplitude for the process (2.11) may be related to the difference of K^0 and $\bar{K}^0$ scattering. (See Eden 1971 for a discussion of this relation and its consequences.)

2.6. *Backward scattering*

For $\pi^+ p$ scattering near to the backward direction in the CM system as shown in figure 14, it is found that there is a backward peak at $\theta = \pi$, and a dip analogous to that seen in figure 13. A similar structure is found in $\pi^- p$ charge-exchange differential cross sections near $\theta = \pi$. However, for $\pi^- p$ scattering, there is a peak at $\theta = \pi$ but no nearby dip is observed. The magnitude of all three differential cross sections at $\theta = \pi$ decreases rapidly as a function of the energy approximately like $s^{-1{\cdot}5}$.

2.7. *Polarization and spin parameters*

Experiments to measure polarization in nucleon–nucleon and pion–nucleon scattering may be done either by using a polarized target or by measuring the final-state polarization through rescattering the proton. Other spin parameters require both the initial and final polarization to be measured. Polarization measurements play an important role both in determining the several scattering amplitudes that may be involved (two for πN, five for NN) and in determining the phases of the amplitudes. They are not easy experiments, and only recently have moderately accurate experiments become feasible.

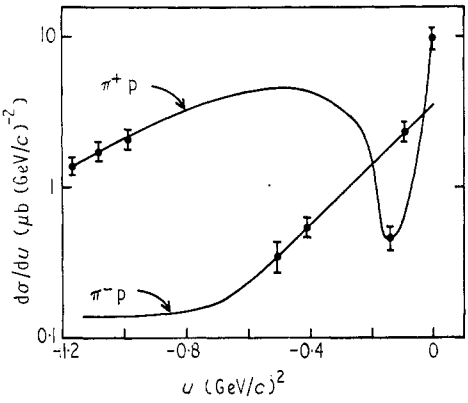

Figure 14. Backward πp scattering at 6·9 (GeV/c) plotted as a function of exchange momentum transfer squared (u) (adapted from Baker *et al* 1968).

2.8. *Large-angle scattering*

At a fixed angle of scattering, as the energy variable s becomes large so also does the momentum transfer variable $|t|$. One would therefore expect the high-energy behaviour to be different in character at fixed angle (traditionally described as large angle) from the behaviour at fixed $|t|$. Experimental results for proton–proton elastic scattering are shown in figure 15 as functions of $|t|$ plotted for various fixed values of the energy ranging from p(lab) = 3 GeV/c to p(lab) = 19 GeV/c. The statistical errors are very little larger than the thickness of the curves in figure 15.

2.9. *Quasi-two-body reactions*

Just as we have previously distinguished elastic scattering and charge-exchange scattering, in the more general case of quasi-two-body reactions we distinguish two classes (i) quasi-elastic reactions or diffraction dissociation and (ii) exchange reactions.

Diffraction dissociation is used to describe processes like

$$\mathrm{p}+\mathrm{p}\rightarrow\mathrm{p}+\mathrm{N}'^{+}(1688) \tag{2.12}$$

in which the final particles each have the same quantum number as the corresponding initial particles except for a possible change in spin and a corresponding change in parity. Thus the reaction (2.12) can take place with an interaction involving an exchange of vacuum quantum numbers carrying angular momentum only.

It is found that integrated diffraction dissociation cross sections remain approximately constant as functions of the energy. Typically they are of the order of 1 mb, or a few per cent of elastic cross sections. Their differential cross sections have a forward peak structure similar in its general features to that discussed for elastic scattering.

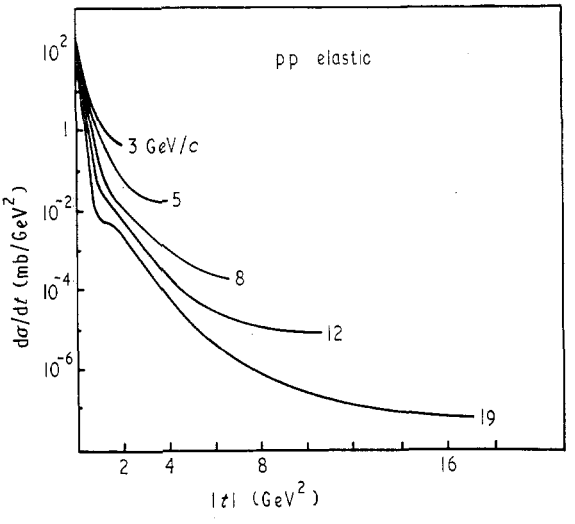

Figure 15. Differential cross sections for pp scattering at various energies (from Allaby *et al* 1968).

Exchange reactions include

$$p + p \rightarrow p + N'^{+}(1236) \tag{2.13}$$

$$\pi^- + p \rightarrow \rho^- + p \tag{2.14}$$

$$\pi^- + p \rightarrow \rho^0 + N'(1236). \tag{2.15}$$

These cannot proceed by exchange of vacuum quantum numbers. It is found that they have the characteristic feature of charge-exchange scattering including a rapid decrease as the energy increases. Their differential cross sections sometimes show a simple forward peak similar to those in figure 10 (but reducing in magnitude with increasing energy), and they sometimes show forward structure similar to that in figure 13.

In quasi-two-body reactions, one or both of the final-state particles decays into two or more particles, and it is the latter that are actually observed experimentally. This means that the polarization is always measured. The corresponding density matrices provide additional tests for any theoretical model of the reactions.

2.10. *Photoproduction*

Photoprocesses have been studied experimentally for γ ray energies up to 16 GeV. The total photoproduction cross section on protons becomes approximately constant at a value around 120 μb above 3 GeV photon energy. Below this energy it shows strong resonances related to those in the πN system.

Photoprocesses include the following typical reactions

$$\gamma p \to \rho^0 p \tag{2.16}$$

$$\gamma p \to \omega p \qquad \gamma p \to \pi^0 p \tag{2.17a}$$

$$\gamma p \to K^+ \Lambda \qquad \gamma p \to \pi^+ n \tag{2.17b}$$

$$\gamma p \to \pi^- \Delta^{++}(1236). \tag{2.17c}$$

The angular distributions and spin correlations for these and other processes have been studied experimentally (see Lohrman 1969 for detailed references). The reaction (2.16) can proceed by exchange of vacuum quantum numbers, and it is therefore analogous to diffraction dissociation. All the reactions (2.17*a*, *b*, *c*) require non-zero quantum numbers to be exchanged.

2.11 *Multiparticle production*

The experimental cross sections for multiparticle production in a bubble chamber are illustrated in figure 16, which shows the proportion of the total cross

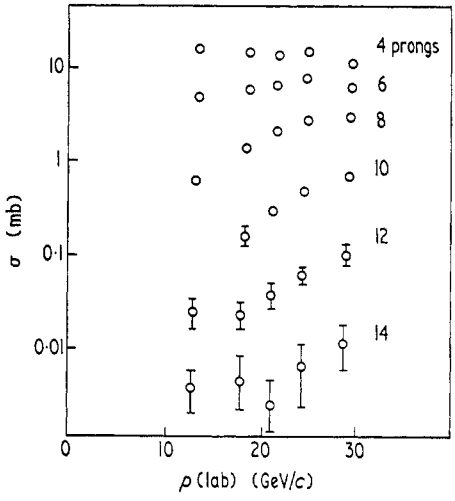

Figure 16. Cross sections for pp collisions defined by the number of (charged particles) prongs in the final state (from Smith *et al* 1970, see also Horn 1972).

section in pp collisions ($\sigma_T \sim 40$ mb) that is due to various numbers of charged particles being produced. It is evident, from the dominance of 4-prong cross sections (4 charged particles) over the remainder, that the mean number of produced charged particles in the final state will be in the region of 4 (allowing for the possibility of neutrals that are not observed directly and subtracting 2 to allow for the initial baryon pair).

The angular distributions of multiparticle production processes may be studied experimentally, and also theoretically by means of Regge models and other models. In particular, the multiplicity and energy distribution of product particles have been extensively studied in a statistical model by Hagedorn and Ranft (1968). Regge theory of multiparticle production, which will be mentioned in a later section, has been recently reviewed by Jacob (1971) and other models have been reviewed by Van Hove (1971).

2.12. *Inclusive reactions*

An inclusive reaction is one in which not all the particles in the final state are observed. The simplest of these gives the total cross section, where none of the final particles is observed but all possible final states are included in the measurement. Then σ(total) will be a function of the energy only.

Considerable attention is currently being given to inclusive reactions in which just one final state particle is observed, for example

$$\mathrm{pp} \rightarrow \pi^- + \text{anything}. \tag{2.18}$$

The corresponding differential cross section may be averaged over the azimuthal angle of the single particle in the final state. It then depends on only two variables if the initial energy of the system is held fixed. Two variables that are often chosen

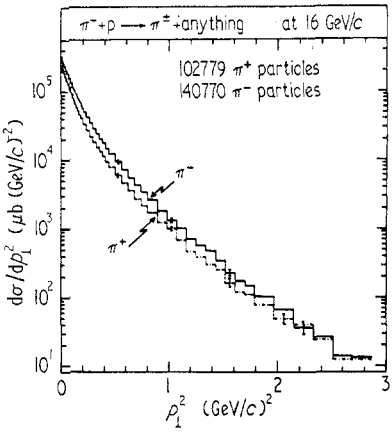

Figure 17. The inclusive reactions $\pi^+ \mathrm{p} \rightarrow \pi^+ + \text{anything}$, and $\pi^- \mathrm{p} \rightarrow \pi^- + \text{anything}$. Distribution as a function of p_T^2 at 16 GeV/c (Van Hove 1971 unpublished) (note $p_T \equiv p_\perp$).

as the independent variables are p_L, the (longitudinal) momentum of the final observed particle in the CM system parallel to the momentum of the incident particle, and p_T (or $p_\perp$) the modulus of the (transverse) momentum of the observed particle perpendicular to the direction of motion if the incident particle. Thus one obtains

$$\frac{\mathrm{d}^2\sigma}{\mathrm{d}p_L\,\mathrm{d}p_T}. \tag{2.19}$$

It is interesting to average over p_L or over p_T and plot the resulting distribution. An example is shown in figure 17, where an average has been taken over p_L and p_T^2 (instead of p_T) is used as the independent variable. The processes in this instance are

$$\pi^- + \mathrm{p} \rightarrow \pi^- + \text{anything} \tag{2.20}$$

$$\pi^+ + \mathrm{p} \rightarrow \pi^+ + \text{anything}. \tag{2.21}$$

It is found that the inclusive cross sections (2.19) have a sharp drop-off as a function of p_T, as is seen in figure 17. The distribution as a function of both p_L

and p_T is shown in a 'Peyrou plot' in figure 18 in which the density of dots indicates the frequency of events. The semicircles bound the regions that are kinematically allowed.

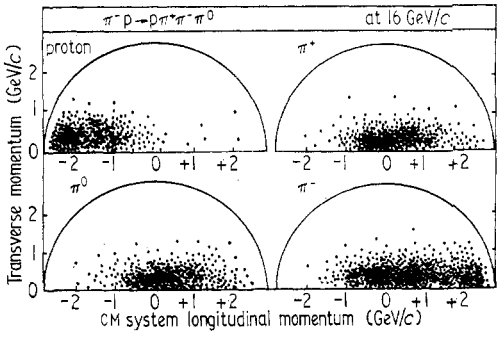

Figure 18. Peyrou plot for $\pi^- p \to p\pi^- \pi^0 \pi^+$ at 16 GeV/c (from Honecker *et al* 1969, see also Horn 1972).

3. Theoretical survey

3.1. *Relativistic kinematics for two-body collisions*

We shall now extend the elementary discussion of kinematics that was introduced in §1.6. There we saw that a scattering amplitude $F(s,t)$ was a function of the invariants s and t. In order to introduce the idea of relativistic crossing symmetry, we now label the incoming and outgoing momenta as in figure 19(a) for the process I

$$\text{I.} \quad a+b \to c+d. \tag{3.1}$$

Thus the outgoing momenta are $-p_c$, $-p_d$, and their energies are $-p_c^0$, $-p_d^0$. Conservation of total energy and momentum requires that

$$p_a+p_b+p_c+p_d = 0. \tag{3.2}$$

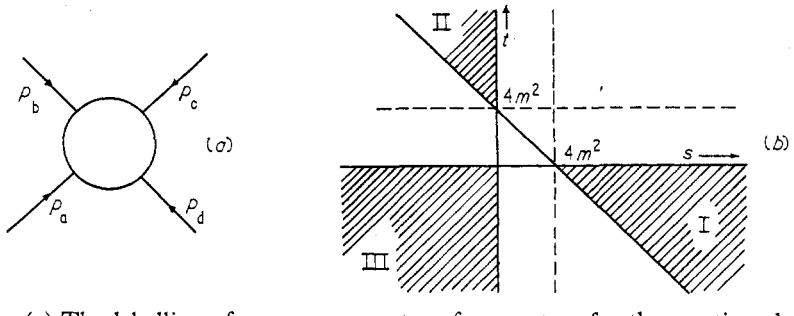

Figure 19. (a) The labelling of energy momentum four-vectors for the reaction ab → cd and crossed reactions. (b) The kinematically allowed physical regions (shown shaded) for equal mass particles in a two-body collision, on an s, t plot where s and t denote the invariant energies squared.

For simplicity we assume that all particles have equal masses m. The mass-shell condition (see equation (1.13)) gives

$$p_a^2 = p_b^2 = p_c^2 = p_d^2 = m^2. \tag{3.3}$$

We define s, t and a third invariant u (minus the exchange momentum transfer squared) by

$$\left.\begin{aligned} s &= (p_a+p_b)^2 \\ t &= (p_b+p_d)^2 \\ u &= (p_b+p_c)^2. \end{aligned}\right\} \tag{3.4}$$

From the conditions (3.2) and (3.3), only two of these variables are independent and

$$s+t+u = 4m^2. \tag{3.5}$$

In the CM system for particles a and b, we write k^2 for the square of the momentum and θ for the scattering angle as in figure 1(b). Then

$$\left.\begin{aligned} s &= 4(m^2+k^2) \\ t &= -2k^2(1-\cos\theta) \\ u &= -2k^2(1+\cos\theta). \end{aligned}\right\} \tag{3.6}$$

The physical values of s and t for process I (equation (3.1)) are shown as the shaded region labelled I in figure 19(b).

The shaded regions marked II and III in figure 19(b) correspond to the values of s and t (or u) for which the following processes are physically allowed:

$$\left.\begin{aligned} &\text{II.} \quad b+\bar{d}\rightarrow\bar{a}+c \\ &\text{III.} \quad b+\bar{c}\rightarrow\bar{a}+d. \end{aligned}\right\} \tag{3.7}$$

For process II, t is the energy squared in the CM system of particles b and $\bar{d}$ (the antiparticle of d); and for III, u is the energy squared of b and $\bar{c}$.

The principle of crossing symmetry asserts that the same scattering amplitude $F(s, t)$ describes all three processes I, II and III provided suitable values of s and t are chosen in each case. This statement applies when the colliding particles have zero spin; more generally, with particles of nonzero spin, several scattering amplitudes are involved in the description of a collision, and the principle of crossing symmetry leads to relations between these amplitudes and those that describe the 'crossed process', that is the process in one of the other physical regions.

For pion–nucleon scattering the kinematics is somewhat more complicated, but we also find there exist scattering amplitudes that relate the following three processes,

$$\left.\begin{aligned} &\pi^+p\rightarrow\pi^+p \\ &\pi^-p\rightarrow\pi^-p \\ &\pi^+\pi^-\rightarrow\bar{p}p. \end{aligned}\right\} \tag{3.8}$$

In this case the physical regions have curved boundaries, the region I being that shown in figure 2.

3.2. *Analyticity and crossing symmetry*

In order to make the principle of crossing symmetry precise, even in the simplest case of identical spinless particles, it is necessary to regard $F(s, t)$ as a function of complex variables s and t. Then F corresponds to a physical amplitude only when these variables take appropriate real values. This involves the study of the analytic properties of the scattering amplitude as a function of these complex variables.

As an illustration of the analytic properties, we shall consider the special case of forward scattering ($t = 0$) for process I, defined above. One finds (for example, from quantum field theory) that the forward amplitude $F(s, 0)$ is an analytic function of the complex variable s throughout the complex s plane, except for branch cuts along the real axis. The complex s plane for $F(s, 0)$ is illustrated in figure 20(a). There is a branch point at the real value,

$$s = (2m)^2 = 4m^2 \tag{3.9}$$

which is the threshold at which process I is a physical process allowed by the kinematic conditions (see also figure 19(b) along the line $t = 0$). There are other

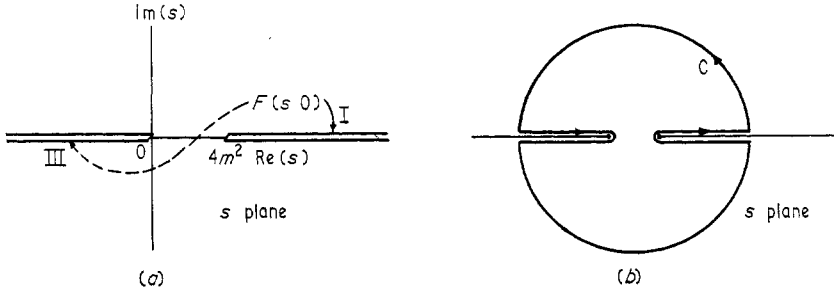

Figure 20. The complex s plane for $t = 0$. (a) Shows the branch cuts along the real axis and the path of analytic continuation from physical region I to physical region III; (b) shows the contour C round which one integrates in order to derive a dispersion relation for the amplitude $F(s, 0)$.

branch points in the s plane, for example at the thresholds for production of new particles, $s = (4m)^2, (6m)^2, \ldots$ in the case of pion–pion scattering. These all lie along the real axis. In addition there are branch points at the corresponding values of u for process III, of which the leading branch point is at $u = 4m^2$. In this case (with $t = 0$) the threshold $u = 4m^2$ corresponds to $s = 0$, and the attached branch cut is drawn along the left-hand real axis.

Between the branch points at $s = 0$ and $s = 4m^2$, the amplitude $F(s, 0)$ is real. This means that the amplitude is hermitian, so that

$$F(s^*, 0) = F^*(s, 0) \tag{3.10}$$

where a star denotes complex conjugation.

The physical amplitude for process I is obtained as indicated in figure 19(a), by taking the limit on top of the right-hand branch cut. When s is real and greater than $4m^2$, we have

$$\text{physical } F(s, 0) = \lim_{\epsilon \to +0} F(s + i\epsilon, 0). \tag{3.11}$$

The physical amplitude for process III, where u is the energy, is obtained in the s plane by taking the limit on to the real axis below the left-hand branch cut. Analytic continuation by the path indicated in figure 19(a) establishes the analytic statement of crossing symmetry, which relates processes I and III, for the forward amplitude. (For further details see Eden *et al* 1966, Martin 1969, Eden 1971 and Roy 1972.)

3.3. *Dispersion relations*

The analytic properties of $F(s,0)$, illustrated in figure 20(a), permit us to derive a dispersion relation provided that $F(s,0)\to 0$ as $|s|\to\infty$ in any direction in the complex s plane. Since $F(s,0)$ is regular inside the closed contour C, shown in figure 20(b) we can use Cauchy's theorem to give

$$F(s,0)=\frac{1}{2\pi i}\int_C \frac{F(s',0)\,ds'}{s'-s}. \tag{3.12}$$

If $F(s,0)\to 0$ as $|s|\to\infty$, we obtain the dispersion relation

$$F(s,0)=\frac{1}{\pi}\int_{4m^2}^{\infty}\frac{ds'\,\mathrm{Im}\,F(s',0)}{s'-s}+\frac{1}{\pi}\int_{-\infty}^{0}\frac{ds'\,\mathrm{Im}\,F(s',0)}{s'-s}. \tag{3.13}$$

In deriving this result, we have used hermitian analyticity which gives (in the limit $\epsilon\to 0$)

$$F(s'+i\epsilon,0)-F(s'-i\epsilon,0)=2i\,\mathrm{Im}\,F(s',0). \tag{3.14}$$

The imaginary part of the forward amplitude can be related to the total cross section, for process I for $s>4m^2$, and for process III for $s<0$, by means of the optical theorem (see equation (1.37)). This permits a relation between $F(s,0)$ for complex s and physically measurable cross sections.

We have seen in figure 5 that total cross sections tend to constant values at large energies. The optical theorem then gives

$$\begin{aligned}\mathrm{Im}\,F(s,0)&=[s(s-4m^2)]^{1/2}\,\sigma(\text{total})\\&\simeq s(\text{constant})\quad \text{as } s\to\infty.\end{aligned} \tag{3.15}$$

This shows that, for the forward amplitude, our assumptions for obtaining a dispersion relation are not correct. However, we can apply Cauchy's theorem instead to the modified amplitude G, defined by

$$s^2\,G(s,0)=F(s,0)-F(0,0)-sF'(0,0) \tag{3.16}$$

where F' denotes the derivative of F at $s=0$.

After applying Cauchy's theorem, we obtain a dispersion relation for F with two subtraction terms,

$$\begin{aligned}F(s,0)=F(0,0)+sF'(0,0)&+\frac{s^2}{\pi}\int_{4m^2}^{\infty}\frac{ds'\,\mathrm{Im}\,F(s',0)}{s'^2(s'-s)}\\&+\frac{s^2}{\pi}\int_{-\infty}^{0}\frac{ds'\,\mathrm{Im}\,F(s',0)}{s'^2(s'-s)}.\end{aligned} \tag{3.17}$$

More generally, it is necessary to consider the amplitude $F(s,t)$ as a function of two complex variables, and in some circumstances one can derive double dispersion relations in both variables simultaneously. The latter were first proposed by Mandelstam (1958) and they are referred to as a Mandelstam representation for the scattering amplitude.

3.4. *Scattering amplitudes and the S matrix*

The S matrix approach to elementary particle physics was proposed by Heisenberg (1943). His idea was to formulate a theory in which the main components (the elements of the S matrix) were almost directly related to experimentally measurable

quantities. An S matrix element is the transition amplitude from an incoming state α to an outgoing state β in any collision process. Formally this gives

$$S_{\beta\alpha} = (\beta, \text{out}\,|\,\alpha, \text{in}) = (\beta, \text{in}\,|\,S\,|\,\alpha, \text{in}). \tag{3.18}$$

Hence it can be seen that S is a unitary matrix. This is related to the collision amplitude $T_{\beta\alpha}$ by

$$S_{\beta\alpha} = \delta_{\beta\alpha} + \mathrm{i}(2\pi)^4\,\delta(\Sigma p_\beta - \Sigma p_\alpha)\,T_{\beta\alpha}. \tag{3.19}$$

The first δ function $\delta_{\beta\alpha}$ corresponds to zero interaction, the second ensures total energy–momentum conservation. With suitably chosen normalization $T_{\alpha\beta}$ is a relativistic invariant. In the particular case of elastic scattering $T_{\alpha\beta}$ is the scattering amplitude $F(s,t)$ and is related to differential cross sections as noted in equation (1.30).

For pion–nucleon scattering taking account of nucleon spin, $T_{\beta\alpha}$ becomes a 4×4 matrix. Then instead of equation (1.30) we get

$$\frac{\mathrm{d}\sigma}{\mathrm{d}\Omega} = \frac{m^2}{16\pi^2 s}\sum_{\text{spin}}|\,\bar{u}_\beta\,T_{\beta\alpha}\,u_\alpha\,| \tag{3.20}$$

where u_α, u_β denote Dirac spinors. The matrix $T_{\beta\alpha}$ is related to two independent scalar amplitudes A and B,

$$T_{\alpha\beta} = A(s,t)\,\delta_{\alpha\beta} - \tfrac{1}{2}\mathrm{i}B(s,t)\,\gamma^\mu_{\alpha\beta}(q_1+q_2)_\mu \tag{3.21}$$

where q_1 and q_2 denote the pion momenta and γ_μ is a Dirac γ matrix.

Instead of the A and B amplitudes, it is often convenient to use the non-spin-flip amplitude $f(s,t)$ and the spin-flip amplitude $g(s,t)$, which are linearly related to A and B. For these amplitudes

$$\sigma_{\mathrm{T}}(s) = \frac{4\pi}{|q_1|}\,\mathrm{Im}\,f(s,t=0) \tag{3.22}$$

$$\frac{\mathrm{d}\sigma}{\mathrm{d}\Omega} = |\,f(s,t)|^2 + |g(s,t)|^2. \tag{3.23}$$

The polarization $P(\theta)$ is given by

$$P(\theta) = 2\,\mathrm{Im}\,[f^* g] \tag{3.24}$$

where f^* is the complex conjugate of f. (For further details about the S matrix see Chew (1966) and Eden *et al* (1966).)

3.5. *Partial wave expansions*

For simplicity we will consider equal mass spinless particles having a single scattering amplitude $F(s,t)$. Its partial wave expansion takes the form

$$F(s,t) = \frac{8\pi W}{k}\sum_{l=0}^{\infty}(2l+1)\,f_l(s)\,\mathrm{P}_l(\cos\theta) \tag{3.25}$$

where $W^2 = s = 4(m^2+k^2)$ and

$$f_l(s) = \frac{1}{2}\int_{-1}^{1}\mathrm{d}(\cos\theta)\,\frac{kF(s,t)}{8\pi W}\,\mathrm{P}_l(\cos\theta). \tag{3.26}$$

The unitarity of the S matrix corresponds to conservation of probability. It leads

to the optical theorem equation (1.37). For partial waves, in the case where only elastic scattering can take place, unitarity takes the form

$$i(f_l^* - f_l) = 2|f_l|^2 \tag{3.27}$$

giving

$$f_l(s) = \frac{\exp(2i\delta_l) - 1}{2i} \tag{3.28}$$

where the phase shift $\delta_l(s)$ is real in the elastic region.

More generally, when inelastic scattering is possible, f_l satisfies

$$0 \leqslant |f_l|^2 \leqslant \operatorname{Im} f_l \leqslant 1. \tag{3.29}$$

Thus

$$f_l(s) = \frac{\eta_l \exp(2i\delta_l) - 1}{2i} \tag{3.30}$$

where δ_l is real and $0 \leqslant \eta_l \leqslant 1$.

3.6. *Resonances and Regge poles*

At a resonance the total cross section becomes large, so that $\operatorname{Im} F(s', 0)$ in the dispersion relation equation (3.17) also becomes large. This may lead to a useful method for approximating the integral in the dispersion relation. More generally, the amplitude $F(s, t)$ will have a pole in the complex variable s, near the real value of s at which the resonance is observed. This pole does not lie in the complex s plane shown in figure 20, but will be found in the second Riemann sheet that is reached through the branch cut. If the resonance corresponds to a state of angular momentum l, the appropriate Legendre polynomial will appear in the residue at the resonance pole; thus near the pole we shall have

$$\frac{k}{8\pi W} F(s, t) \simeq \frac{g P_l(\cos\theta)}{s - a(s) + ib(s)} \tag{3.31}$$

where $a(s)$ and $b(s)$ vary slowly with s and

$$\cos\theta = 1 + 2t/(s - 4m^2). \tag{3.32}$$

It is frequently convenient to analyse the amplitude as a partial wave series; indeed this is how resonances are derived from experimental differential cross sections. The above resonance would occur as a pole in the partial wave amplitude f_l corresponding to angular momentum l,

$$f_l(s) = \frac{1}{2}\int_{-1}^{1} d(\cos\theta) \frac{k}{8\pi W} F(s, t(\theta)) P_l(\cos\theta). \tag{3.33}$$

Near $s = a - ib$, we shall have a resonance pole, and

$$f_l(s) \simeq \frac{g}{s - a + ib}. \tag{3.34}$$

It should be noted that a and b are both dependent on l as well as on s. Writing

$$a - ib = s_0(l, s) \tag{3.35}$$

(3.34) becomes

$$f_l(s) \simeq \frac{g}{s - s_0(l, s)}. \tag{3.36}$$

For nonrelativistic scattering on a Yukawa potential, Regge (1959) showed that a unique analytic extension $f(l, s)$ could be defined such that at integer values it is equal to the partial wave amplitude,

$$f(l, s) = f_l(s) \quad (l = 0, 1, 2, \ldots). \tag{3.37}$$

Using Regge's analytic extension, the location $s_0(l, s)$ of the resonance pole in equation (3.36) becomes an analytic function. One can then solve the equation

$$s = s_0(l, s) \tag{3.38}$$

to give

$$l = \alpha_0(s). \tag{3.39}$$

This permits equation (3.36) to be rewritten giving

$$f(l, s) = \frac{r}{l - \alpha_0(s)}. \tag{3.40}$$

Now the pole in the (extended) partial wave amplitude is located in the complex l plane and its position is a function of s. This is called a Regge pole, and the path that it follows as s moves through real values is called a Regge trajectory. We will return to these topics in more detail in § 4, where our main purpose is to show that for large values of t (the energy in channel II of figure 19(b)) Regge theory indicates that a scattering amplitude may have the asymptotic behaviour,

$$F(s, t) \sim C(s)\,(t/t_0)^{\alpha(s)} \tag{3.41}$$

where $\alpha(s)$ denotes the location of a Regge pole associated with a resonance in the channel I of figure 19(b) (where s is the energy).

4. Basic ideas in Regge theory

In this section we shall begin by stating in a general way the main objectives of the Regge pole model. Firstly we shall indicate how a Regge trajectory may correlate sequences of particles and resonances. Secondly we will indicate how the model predicts that high-energy (quasi) two-body reactions are dominated by certain exchanged trajectories. With these two objectives in mind we will then outline the manner in which they may be achieved in a mathematical derivation provided certain assumptions are made.

4.1. *Regge trajectories and sequences of particles*

The Regge pole model states that there exist (complex) Regge trajectory functions $\alpha_n(s)$, depending on $s = W^2$ (the square of the centre of mass energy), that correlate certain sequences of particles or resonances. In relativistic theory the particles associated with a given function $\alpha_n(s)$ have the same internal quantum numbers (baryon number, isospin, parity, strangeness, etc.) but they have spins that differ by units of two. In nonrelativistic potential scattering a given function $\alpha_n(s)$ correlates sequences of bound states or resonances, and, in the absence of exchange forces, the spins (angular momenta) will differ by only one unit.

We will begin with the example given by the nucleon (neutron or proton) N(938) which has isospin $\frac{1}{2}$, parity $+$, and spin $\frac{1}{2}$. There are resonances, N(1688) and N(2220), in the πN system, that have spin $\frac{5}{2}$ and $\frac{9}{2}$, respectively, and have the

same isospin ($\frac{1}{2}$) and parity ($+$) as the nucleon. The Regge pole model asserts that the nucleon trajectory function $\alpha_N(s)$ satisfies

$$\left.\begin{aligned} &\mathrm{Re}\,\alpha_N(s=(0{\cdot}938)^2)=\tfrac{1}{2}\\ &\mathrm{Re}\,\alpha_N(s=(1{\cdot}688)^2)=\tfrac{5}{2}\\ &\mathrm{Re}\,\alpha_N(s=(2{\cdot}220)^2)=\tfrac{9}{2}. \end{aligned}\right\} \tag{4.1}$$

The corresponding Regge trajectory is illustrated by the full line in figure 21(*a*) which shows a Chew–Frautschi plot of $\mathrm{Re}\,\alpha_N$ as a function of the energy squared s

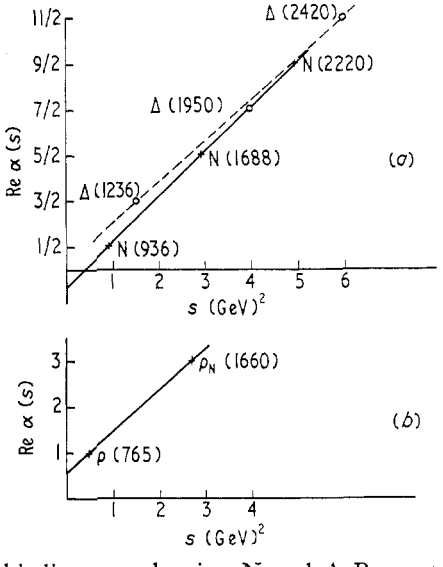

Figure 21. Chew–Frautschi diagrams showing N and Δ Regge trajectories in (*a*) and the probable ρ trajectory in (*b*).

measured in GeV². It will be observed from figure 21(*a*) that the trajectory is nearly a straight line, thus with s in GeV²,

$$\mathrm{Re}\,\alpha_N(s)\simeq\alpha_N^0+\alpha_N' s. \tag{4.2}$$

In particular

$$\alpha_N^0\simeq -0{\cdot}37 \qquad \alpha_N'\simeq 1{\cdot}0\ \mathrm{GeV}^{-2}. \tag{4.3}$$

Another Regge trajectory is illustrated by a sequence associated with the Δ(1236). This is also a resonance in the πN system but it has isospin $\frac{3}{2}$, and spin–parity $(\frac{3}{2})^+$, so it cannot be associated with the nucleon Regge trajectory since an internal quantum number (isospin) is different (also its spin differs by only one unit from that of N(938)).

The other resonances associated with the Δ(1236) (see figure 7) are the Δ(1950) and the Δ(2420) which have spin $\frac{7}{2}$ and $\frac{11}{2}$, respectively, while their other quantum numbers are the same as the Δ(1236), namely isospin $\frac{3}{2}$, parity $+$, baryon number 1, strangeness 0. The corresponding Regge trajectory $\alpha_\Delta(s)$ is illustrated by the broken line in figure 21(*a*). It has

$$\left.\begin{aligned} &\alpha_\Delta(s=(1{\cdot}236)^2)=\tfrac{3}{2}\\ &\alpha_\Delta(s=(1{\cdot}950)^2)=\tfrac{7}{2}\\ &\alpha_\Delta(s=(2{\cdot}420)^2)=\tfrac{11}{2}. \end{aligned}\right\} \tag{4.4}$$

Writing

$$\alpha_\Delta(s) = \alpha_\Delta^0 + \alpha_\Delta' s \tag{4.5}$$

we obtain

$$\alpha_\Delta^0 \simeq 0{\cdot}15 \qquad \alpha_\Delta' \simeq 0{\cdot}9 \text{ GeV}^{-2}. \tag{4.6}$$

Thus the slopes of α_Δ and α_N are approximately equal,

$$\alpha_\Delta' \simeq \alpha_N' \simeq 1{\cdot}0 \text{ GeV}^{-2}. \tag{4.7}$$

As a third example we take the $\rho(765)$ meson Regge trajectory, but instead of deriving α_ρ' we will assume that it takes the same value noted in equation (4.7). Then,

$$\alpha_\rho(s) \simeq \alpha_\rho^0 + s. \tag{4.8}$$

Since the ρ meson has $(\text{mass})^2 = 0{\cdot}5 \text{ GeV}^2$ and spin 1, we find from (4.8) that $\alpha_\rho^0 \simeq 0{\cdot}5$ giving

$$\alpha_\rho(s) \simeq 0{\cdot}5 + s \tag{4.9}$$

which is illustrated in figure 20(*b*).

The next resonance on the ρ trajectory should have spin 3. Writing $\alpha_\rho(s) = 3$, we obtain a mass

$$m = s^{1/2} = (2{\cdot}5)^{1/2} \simeq 1{\cdot}6 \text{ GeV}. \tag{4.10}$$

If the idea of linearity of Regge trajectories is correct, there should therefore be a meson resonance having spin 3, mass approximately 1600 MeV, and having its other quantum numbers (isospin 1, G-parity +) the same as the $\rho(765)$. A candidate has indeed been observed; the $\pi\pi$ resonance $\rho_N(1660)$ has isospin 1 and G-parity +, and its spin has recently been measured by Hyams *et al* (1971), who find a value 3 in agreement with the ρ Regge trajectory, drawn in figure 21(*b*).

4.2. *Exchanged trajectories and high-energy behaviour*

In §4.1 we have illustrated the first main feature of the Regge pole model, namely the existence of trajectories $\alpha(s)$ such that whenever $s = m_r^2$ (where m_r is the mass of a particle in the trajectory), then $\alpha(m_r^2) = J_r$ (the spin of the particle). The spins of particles on the same trajectory differ by two units.

The second main feature of the Regge pole model is the relation between exchanged trajectories and high-energy behaviour. We will illustrate this by the charge-exchange reaction

$$\pi^- p \to \pi^0 n \qquad (s \text{ channel}). \tag{4.11}$$

We call this the s channel to denote that s is the invariant energy squared. Then the t channel, as defined in §3.1, will be

$$p\bar{n} \to \pi^+ \pi^0 \qquad (t \text{ channel}). \tag{4.12}$$

The elastic cross section for $\pi^+\pi^0$ has a resonance at 765 MeV, namely the ρ^+ meson. This resonance may also be pictured as a bound state of the $p\bar{n}$ system. Thus it is a resonance (bound state) in the process (4.12). As noted in §4.1, there is a Regge trajectory associated with this resonance, but in this case it is a function of t,

$$\alpha_\rho(t). \tag{4.13}$$

The existence of this exchanged ρ trajectory is indicated schematically in figure 22(*a*). It is common practice to label the exchanged trajectory with the same symbol as the leading particle on the trajectory, in this case the ρ meson. The exchanged object is also called a Reggeon to distinguish it from models in which elementary particles are exchanged. An important feature about an exchange diagram like figure 22(*a*) is that quantum numbers (charge, strangeness, baryon number, etc, except spin) must be conserved at the vertices where the Reggeon meets the lines representing the incoming and outgoing particles.

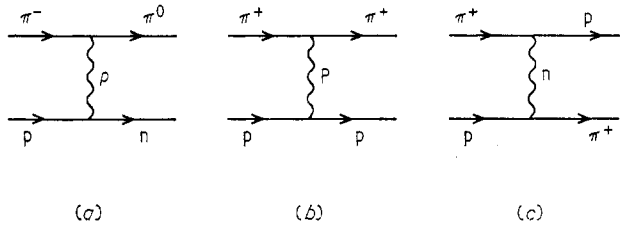

Figure 22. Regge exchange diagrams illustrating: (*a*) exchange of a ρ meson trajectory in pion–nucleon charge exchange, (*b*) Pomeron exchange in elastic πp scattering and (*c*) neutron exchange in backward π^+ p scattering.

Given all allowed exchange diagrams for the process (4.11), the Regge pole model instructs one to choose the diagram in which $\mathrm{Re}\,\alpha(t)$ is largest, in this case figure 22(*a*). Then the Regge pole model predicts that the high-energy behaviour of the charge exchange differential cross section is given by

$$\frac{\mathrm{d}\sigma(\pi^- \mathrm{p} \to \pi^0 \mathrm{n})}{\mathrm{d}t} \sim |b(t)|^2 s^{2\alpha(t)-2}. \tag{4.14}$$

It is evident that for high energies (large s), the second factor will change much faster as a function of t than any given function $b(t)$, so let us assume $b(t) \simeq b_0$ if $|t|$ is not large. Using equation (4.8) with t instead of s, (4.14) becomes

$$\frac{\mathrm{d}\sigma}{\mathrm{d}t} \sim |b_0|^2 s^{2\alpha_\rho^0 - 2} \exp(2\alpha'_\rho t \ln s) \tag{4.15}$$

where $\alpha_\rho^0 = 0{\cdot}5$ and $\alpha'_\rho = 1$. Integrating over t we obtain

$$\sigma_{\mathrm{ex}}(\pi^- \mathrm{p} \to \pi^0 \mathrm{n}) \sim \frac{|b_0|^2}{s 2\alpha'_\rho \ln s}. \tag{4.16}$$

Thus

$$\ln(\sigma_{\mathrm{ex}}) \sim \text{constant} - \ln s - \ln(\ln s). \tag{4.17}$$

This result compares favourably with the experimental values given in figure 12 (recall that $\ln s \simeq \ln(p(\mathrm{lab}))$ at high energies). This gives support to the value $\alpha_\rho^0 = 0{\cdot}5$, which was deduced in §4.1 by guessing that $\alpha'_\rho = 1\ \mathrm{GeV}^{-2}$.

In figure 22(*b*) we illustrate an elastic scattering process in which the exchanged Reggeon carries no internal quantum numbers. The corresponding Reggeon is called the Pomeron (or Pomeranchon) after Pomeranchuk who was the first to suggest that a total cross section should tend to a constant at high energies. The Pomeron trajectory has the form

$$\alpha_{\mathrm{P}}(t) = 1{\cdot}0 + \alpha'_{\mathrm{P}} t. \tag{4.18}$$

It follows from the optical theorem, equation (1.37), and §5.2, that the value 1·0 given for α_P^0 ensures that $\sigma(\text{total}) \to \text{constant}$.

In figure 22(*c*) we illustrate the exchange of a nucleon N (or baryon N*). In near-backward πN scattering the nucleon N, or the resonance N*, are treated as Reggeons that dominate for large s, at fixed u (the exchange momentum transfer squared).

4.3. *Extended partial wave amplitudes and Regge poles*

We turn now to an outline of the mathematical derivation of the results stated in the previous two subsections. Regge's original paper (1959) studied the scattering of a particle on a Yukawa potential. In that case many results can be proved that will be stated here as assumptions. Many of these assumptions cannot be proved in relativistic collisions although some of them can be made plausible (see, for example, the book by Collins and Squires 1968). Others are guessed by analogy with potential scattering, or are made purely for simplicity in an attempt to obtain a first approximation to a theory of strong interactions (as in Regge pole models).

We begin with the partial wave series for equal mass collisions in the t channel (so t is the energy squared). Then, denoting the CM system momentum by k and scattering angle by θ, we have

$$t = 4(k^2 + m^2) \tag{4.19}$$

$$s = -2k^2(1 - \cos\theta) \tag{4.20}$$

$$F(s,t) = \frac{8\pi t^{1/2}}{k} \sum_0^\infty (2l+1)\, f_l(t)\, \mathrm{P}_l(\cos\theta). \tag{4.21}$$

This series can be shown to converge if $\cos\theta$ is inside a certain ellipse, with foci at -1 and $+1$. The ellipse extends along $\cos\theta$ real to a value that corresponds to $s = 4m^2$ (see equation (4.20)). In order to obtain a form of $F(s,t)$ that converges even when s is large ($\cos\theta$ large), Regge made use of the Sommerfeld–Watson transform which we will consider in §4.4. This method requires an extension of the partial wave amplitude $f_l(t)$, which is needed in (4.21) only for integer l, to a function $f(l,t)$, where l may take complex values, such that

$$f(l,t) = f_l(t) \qquad (l = 0, 1, 2, \ldots). \tag{4.22}$$

This analytic extension can be made uniquely in potential scattering, provided certain restrictions are made on the rate of increase of $|f(l,t)|$ as $|l| \to \infty$. Indeed, for coulomb scattering the partial wave amplitude can be evaluated explicitly and is found to have the form

$$f(l,k) = \frac{1}{2\mathrm{i}}\left[\frac{\Gamma(l+1-\mathrm{i}e^2/2k)}{\Gamma(l+1+\mathrm{i}e^2/2k)} - 1\right]. \tag{4.23}$$

A gamma function $\Gamma(z)$ is regular except at poles at the negative integers and zero. Hence, $f(l,k)$ given by equation (4.23) will be regular except for poles given by

$$l + 1 - \mathrm{i}e^2/2k = -n \qquad (n = 0, 1, 2, \ldots). \tag{4.24}$$

This determines the Regge trajectory $\alpha_n(k)$:

$$l = \alpha_n(k) = -n - 1 + \frac{\mathrm{i}e^2}{2k}. \tag{4.25}$$

The term 'Regge trajectory' is used both for (*a*) the path in the l plane of $\alpha_n(k)$, moving as a function of $E = k^2$ and for (*b*) $\mathrm{Re}\,\alpha_n(k)$ plotted against $E = k^2$. The latter is the analogue of the Regge trajectories shown in figure 21. Coulomb Regge trajectories are shown in figure 23, both for type (*a*) and for type (*b*).

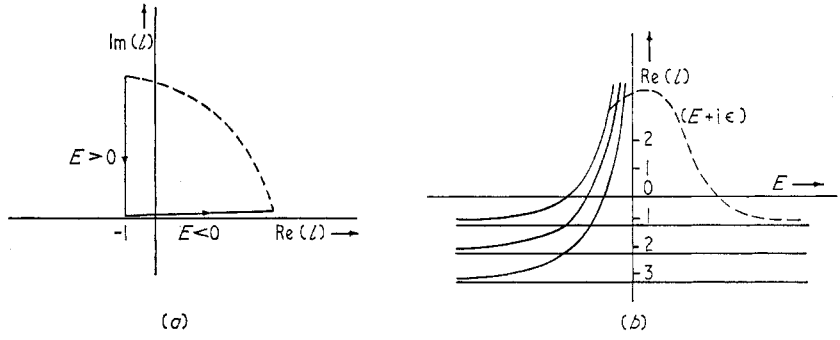

Figure 23. Regge trajectories for an attractive coulomb potential, (*a*) the path of the leading coulomb Regge pole $l(E)$ as E varies from $-\infty$ to $+\infty$; (*b*) the projection on to the (real l, real E) plane of coulomb Regge poles; the broken line shows how the projection of a pole moves as E avoids the singular point $E = 0$ in going from negative to positive values.

When $\alpha_n(k)$, given by equation (4.25), takes a positive integer value, l corresponds to a physical value l_0 of angular momentum and represents a bound state in an attractive coulomb potential. Thus (4.25) determines the energies of bound states for $l = l_0$,

$$E_{l_0} = k^2 = -\frac{e^4}{4(l_0+n+1)}. \tag{4.26}$$

These are the well-known coulomb levels and they establish, in this example, the results stated without proof in § 4.1. It has been proved by Regge (1959, 1960) that similar results hold for scattering by a Yukawa potential.

In relativistic S matrix theory, it is also possible to define analytic extensions of the partial wave amplitude $f_l(t)$ but it turns out that it is necessary to make separate extensions $f^+(l,t)$ and $f^-(l,t)$ of the even and odd partial waves. Thus

$$f^+(l,t) = f_l(t) \qquad (l = 0, 2, 4, \ldots) \tag{4.27}$$

$$f^-(l,t) = f_l(t) \qquad (l = 1, 3, 5, \ldots). \tag{4.28}$$

Then the even signature partial wave amplitude $f^+(l,t)$ has poles

$$l = \alpha_n^+(t). \tag{4.29}$$

Only when $\alpha_n^+(t)$ is an even integer (or zero) will this even signature trajectory correspond to a physical particle. Similarly the odd signature trajectory function $\alpha_m^-(t)$ must equal an odd integer when t is the mass squared of a physical particle.

We can now express the relation to bound state or resonance poles in $f_l(t)$ more precisely than was done in § 3.6. Let us suppose that $f_{l_0}(t)$ (l_0 even) has a pole at $t = t_0$, which corresponds to a bound state (t_0 real) or a resonance ($t_0 = a - ib$). Near $t = t_0$, we can expand $\alpha_n^+(t)$:

$$\begin{aligned}\alpha_n^+(t) &\simeq \alpha_n^+(t_0) + (t-t_0)\,\alpha_n^+(t_0) \\ &\simeq l_0 + (t-t_0)\,\alpha_0'.\end{aligned} \tag{4.30}$$

Thus, for l near l_0 and t near t_0, the amplitude will have the form

$$f^+(l,t) \simeq \frac{R}{l-l_0-(t-t_0)\alpha_0'}$$

$$\simeq \frac{R/\alpha_0'}{(l-l_0)/\alpha_0'+t_0-t}. \tag{4.31}$$

Thus, when $l = l_0$ we have a bound state, pole or Breit–Wigner resonance pole in $f^+(l_0, t) = f_{l_0}(t)$ at $t = t_0$. Also, when $t = t_0$ we have a Regge pole at $l = l_0$ in $f^+(l, t_0)$.

It has been proved for Yukawa potentials, and it is plausible in general, that Regge trajectories $\alpha_n^+(t)$, $\alpha_n^-(t)$, become complex when t is above the lowest physical threshold ($t = 4m^2$, for equal masses). For $t < 4m^2$, it is often assumed for simplicity that the trajectory functions are real but this result is not always true in potential scattering and is not likely to be true in general.

For Yukawa potential scattering, Regge trajectories $l = \alpha(s)$ can be numerically calculated from the Schrödinger equation. They are not even approximately linear for a simple attractive Yukawa potential, but one could construct a superposition of these potentials which was linear for low values of s. The idea that $\alpha(s)$ may be approximately linear in s was suggested by the experimental results, especially those on nucleon resonances, some of which were discussed in § 4.1.

4.4. *Partial wave series and the Sommerfeld–Watson transform*

For simplicity, we will illustrate the transformation of the partial wave series (4.21) without taking account of the odd and even signature extensions of $f_l(s)$. After completing the transformation we will include the effects of odd and even signature in the result. We begin with (4.21) which we re-write here, with $z = \cos\theta = \{1+2s/(t-4m^2)\}$,

$$F(s,t) = \frac{8\pi t^{1/2}}{k} \sum_0^\infty (2l+1)\, f_l(t)\, \mathrm{P}_l(z). \tag{4.32}$$

Let $f(l, t)$ be the analytic extension of $f_l(t)$, and for simplicity we will assume that it is regular, in the half-plane $\mathrm{Re}\, l > -\frac{1}{2}$, except for complex poles (the Regge pole model). One can show that these poles will be in $\mathrm{Im}\, l \geqslant 0$, as illustrated in figure 24(a).

The procedure for the Sommerfeld–Watson transform begins by re-writing the series (4.32) in the form of an integral round the path C shown in figure 24(a).

$$F(s,t) = \frac{1}{2\pi \mathrm{i}} \int_C g(l)\, \mathrm{d}l \tag{4.33}$$

where

$$g(l) \equiv \frac{8\pi t^{1/2}}{k} \left(\frac{\pi(2l+1)\, f(l,t)\, \mathrm{P}_l(-z)}{\sin \pi l} \right). \tag{4.34}$$

The poles of $g(l)$ inside the contour C in figure 24(a) at $l = 0, 1, 2, \ldots$ arise from the zeros of $\sin \pi l$. The sum of the residues at all these poles leads directly to the partial wave series given in equation (4.32). If $f(l, t)$ happens to have a real pole, one can detour round it as indicated in figure 24(a). Choice of t can ensure that $f(l, t)$ has no poles at integers.

The second stage of the Sommerfeld–Watson transformation consists of using Cauchy's theorem on the closed contour shown in figure 24(*b*).

$$\frac{1}{2\pi i}\int_{(CC'C'')} g(l)\,dl = \sum_n (\text{residue of } g(l) \text{ at } l = \alpha_n). \tag{4.35}$$

The poles of $g(l)$ at $l = \alpha_n(t)$ arise solely from the poles of $f(l, t)$. Using (4.35) we can rewrite (4.33) in the form

$$F(s,t) = \frac{-1}{2\pi i}\int_{C''} g(l)\,dl - \frac{1}{2\pi i}\int_{C'} g(l)\,dl - \frac{8\pi t^{1/2}}{k}\sum_n \frac{\pi(2\alpha_n+1)\,r_n\,P_{\alpha_n}(-z)}{\sin(\pi\alpha_n)} \tag{4.36}$$

where $\alpha_n(t)$ indicates one of the Regge poles of $f(l, t)$ illustrated in figure 24, and the sum is over poles to the right of C″, which is taken along $\operatorname{Re} l = -\frac{1}{2}$.

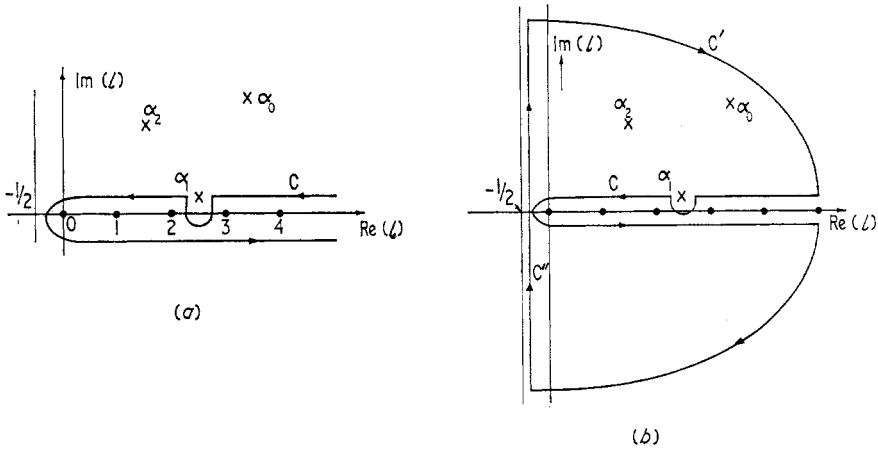

Figure 24. (*a*) The choice of the path C in equation (4.33), Regge poles α_0, α_1, α_2, are illustrated. (*b*) The closed contour C + C′ + C″ giving the result (4.35).

It can be made plausible that the integral along C′ in (4.36) tends to zero as the radius of the semicircle C′ tends to infinity. We note that z and s are related by equation (4.20), namely,

$$z = 1 + \frac{s}{2k^2} = 1 + \frac{2s}{t-4m^2}. \tag{4.37}$$

Thus if $s \to \infty$ for fixed t, we have $z \to \infty$. For large z,

$$|P_\alpha(-z)| \sim |z|^{\operatorname{Re}\alpha}. \tag{4.38}$$

Therefore the right-hand side of equation (4.36) should be dominated, for large s (large z), by the pole $\alpha_0(t)$ for which $\operatorname{Re}\alpha$ is largest. If we order the $\alpha_n(t)$ so that

$$\operatorname{Re}\alpha_0 > \operatorname{Re}\alpha_1 > \operatorname{Re}\alpha_2 > \ldots \tag{4.39}$$

we obtain the following form for $F(s, t)$ given by (4.36) when t is fixed and s is large (note that equation (4.19) fixes k when t is fixed),

$$F(s,t) \sim \sum_n \frac{\beta_n(t)\,(-1)^{\alpha_n}}{\sin(\pi\alpha_n(t))}\left(\frac{s}{s_0}\right)^{\alpha_n(t)} + B(s,t) \tag{4.40}$$

where

$$\beta_n(t) = -\left(\frac{8\pi t^{1/2}}{k}\right)\frac{\pi(2\alpha_n+1)\,r_n(s_0)^{\alpha_n}}{(t-4m^2)^{\alpha_n}} \tag{4.41}$$

s_0 is an arbitrary scale factor and $B(s,t)$ in equation (4.40) denotes a 'background' term, which is assumed to be relatively small as $s\to\infty$ for fixed t in the Regge pole model.

A relativistic theory should take account of the separation of odd and even partial waves in (4.32) before making the transformations. This modifies the result (4.40), and instead it leads to the following asymptotic form for fixed t as $s\to\infty$,

$$F(s,t)\sim\sum_n \frac{\beta_n^+(t)\exp\{i\pi(1-\frac{1}{2}\alpha_n^+)\}}{\sin(\frac{1}{2}\pi\alpha_n^+)}\left(\frac{s}{s_0}\right)^{\alpha_n^+} + \sum_m \frac{\beta_m^-(t)\exp\{i\pi(\frac{1}{2}-\frac{1}{2}\alpha_m^-)\}}{\cos(\frac{1}{2}\pi\alpha_m^-)}\left(\frac{s}{s_0}\right)^{\alpha_m^-} + B(s,t). \tag{4.42}$$

The first term on the right of (4.42) corresponds to even signature Regge poles, the second to odd signature, the third denotes background effects.

The asymptotic form (4.42) illustrates the main predictions of the Regge pole model, and we will consider some of its simpler consequences in the next section. If the formula (4.42) for $F(s,t)$ is substituted into the differential cross section formula equation (1.30), one obtains the result of the Regge pole model that was stated in § 4.2, equation (4.14).

4.5. *Branch cuts in the angular momentum plane*

Regge branch cuts are now regarded as essential both for consistency in Regge theory and for phenomenological applications. These cuts arise from branch-point singularities of the extended partial wave amplitude $f^+(l,s)$ or $f^-(l,s)$. The original assumption of Regge pole models, that the only singularities in $\mathrm{Re}\,l > -\frac{1}{2}$ are simple poles, was made on the basis of potential scattering from a Yukawa potential. The resemblance between this type of potential scattering and relativistic quantum field theory is suggested by considering a sum of the sequence of Feynman diagrams illustrated in figure 25(*a*). The sum of the Feynman integrals corresponding to this infinite sequence of 'ladder' diagrams is illustrated symbolically in figure 25(*b*).

Yukawa potential scattering (Regge 1959, 1960) leads to extended partial wave amplitudes $f(l,s)$ having only simple poles in $\mathrm{Re}\,l > -\frac{1}{2}$. The same result holds for ladder diagrams (Polkinghorne 1963, Federbush and Grisaru 1963). However, the combination of ladder diagrams shown in figure 25(*c*) leads to a branch point in $f(l,s)$ and there are general consistency arguments to show that such branch points are essential to Regge theory (Mandelstam 1963).

General rules can be obtained for the asymptotic behaviour of ladder diagrams and also of more complicated diagrams (Eden *et al* 1966). For certain classes of diagrams it is found that there is cancellation between their branch-cut contributions. However, diagrams like that shown in figure 25(*c*) lead to branch cuts that are not cancelled. The corresponding leading asymptotic behaviour (Landshoff and Polkinghorne 1969) has the form, as $s\to\infty$,

$$F_{\mathrm{cut}}(s,t)\sim B_{\mathrm{cut}}(t)\left(\frac{s}{s_0}\right)^{\alpha_c(t)}\left\{\ln\left(\frac{s}{s_1}\right)\right\}^{-1-\delta(t)}. \tag{4.43}$$

This may be be compared with the simple pole terms shown in equation (4.40). The branch-cut nature of the singularity leads to the contour in the l plane shown in figure 25(d), and in particular to the extra factor in (4.43) involving $\ln(s/s_1)$, where s_1 is another unknown scale parameter.

The analysis of branch cuts also requires separation into even and odd signature partial waves, which affect the phase factors. Thus, for even signature branch cuts (4.43) has the form

$$F_{\text{cut}}(s,t) \sim B'_{\text{cut}}(t) \exp\{i\pi(1-\tfrac{1}{2}\alpha_c)\} \left(\frac{s}{s_0}\right)^{\alpha_c} \left\{\ln\left(\frac{s}{s_1}\right) - \tfrac{1}{2}i\pi\right\}^{-1-\delta(t)}. \tag{4.44}$$

In practice the logarithmic terms in branch-cut contributions to Regge theory can probably be approximated by Regge pole terms in many situations (but not all).

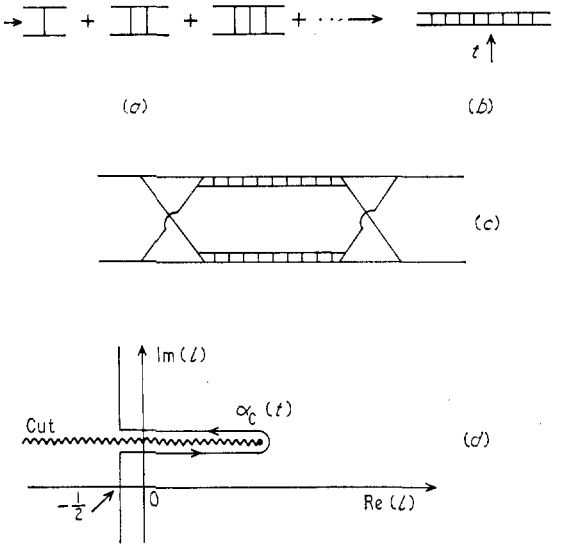

Figure 25. (a) Ladder diagram leading to the Regge pole indicated in (b), (c) a diagram giving a Mandelstam–Regge branch cut and (d) the resulting contour of integration round a branch cut in the l plane.

We will therefore discuss Regge phenomenology mainly in terms of Regge poles. The latter may be 'genuine' and correspond to particles (as discussed in § 4.1), or they may be 'effective' poles that approximate the effects of branch cuts. This situation is unfortunate, since it means that there is not a unique correspondence between the two aspects of Regge theory described in §§ 4.1 and 4.2, respectively. Such a correspondence could be re-established if a unique method was discovered for evaluating the discontinuities across Regge branch cuts.

5. Applications of Regge pole models

In this section we begin with a preliminary summary of the properties of a Regge pole model. We shall then proceed by comparing the model with experimental results. In the course of these comparisons, we shall introduce more features of Regge pole models and shall indicate some of the difficulties that arise.

5.1. *Preliminary summary of properties*

(i) Regge trajectories $\alpha_n^+(t)$ and $\alpha_n^-(t)$ correlate groups of particles (stable particles or resonances) having the same internal quantum numbers (baryon number, isospin, strangeness, parity, etc) but having angular momenta that differ by multiples of two units. Examples of trajectories were given in figure 21.

(ii) The trajectories are such that for $\alpha_n^+(t)$ when $t = m^2$ (m being the mass of a particle on the trajectory of angular momentum J),

$$\alpha_n^+(t = m^2) = J \tag{5.1}$$

for an even signature trajectory, and similarly

$$\alpha_n^-(t = m^2) = J \tag{5.2}$$

for an odd signature trajectory (see §4.4).

(iii) The high-energy behaviour in the s channel as $s \to \infty$, at fixed t, is dominated by the trajectories $\alpha_0^{\pm}(t), \alpha_1^{\pm}(t), \ldots$ having the largest real parts. This gives equation (4.42) which we repeat here for ease of reference

$$F(s,t) \sim \sum_n \frac{\beta_n^+(t) \exp\{i\pi(1-\frac{1}{2}\alpha_n^+)\}}{\sin(\frac{1}{2}\pi\alpha_n^+)} \left(\frac{s}{s_0}\right)^{\alpha_n^+} + \sum_m \frac{\beta_m^-(t) \exp\{i\pi(\frac{1}{2}-\frac{1}{2}\alpha_m^-)\}}{\cos(\frac{1}{2}\pi\alpha_m^-)} \left(\frac{s}{s_0}\right)^{\alpha_m^-} + B(s,t). \tag{5.3}$$

The background term B is assumed to be small. The residues $\beta_n^+(t)$ are assumed to change slowly but they must have zeros when $\alpha_n^+(t) = -2, -4$, etc. Similarly $\beta_m^-(t)$ must be zero when $\alpha_m^-(t) = -1, -3$, etc. If these zeros did not occur, the amplitude (5.3) would be singular for $\alpha(t)$ equal to a negative integer and such unphysical singularities should not be present. The singularities for $\alpha(t)$ equal to positive integers are physical and correspond to the resonance poles in the partial wave amplitudes that give rise to the Regge trajectories. The negative integers are called 'nonsense values' of $\alpha_n(t)$.

(iv) Branch cuts in the l plane give terms like that in equation (4.44) which are additional to the terms shown in equation (5.3).

(v) The residues $\beta_n^+(t)$, or $\beta_m^-(t)$, are sometimes assumed to be zero at all negative integers (and when $\alpha_m^-(t) = 0$). At 'right signature' points these are the zeros noted in (iii) above. At 'nonsense wrong signature' points (eg $\alpha_n^+(t) = -1$, or $\alpha_m^-(t) = 0$) these zeros will make the corresponding term in (5.3) equal to zero.

5.2. *Total cross sections and the Pomeron trajectory*

Consider any elastic scattering amplitude $F(s,t)$ and at $t = 0$ take only the leading pole in (5.3) (ie the one with the largest real part) of even signature,

$$F(s,0) \sim \frac{\beta_0^+ \exp\{i\pi(1-\frac{1}{2}\alpha_0^+)\}}{\sin(\frac{1}{2}\pi\alpha_0^+)} \left(\frac{s}{s_0}\right)^{\alpha_0^+}. \tag{5.4}$$

From the optical theorem (equation (1.37))

$$\begin{aligned} \operatorname{Im} F(s,0) &\sim 2ks^{1/2}\sigma_T(s) \\ &\sim s\sigma_T(s). \end{aligned} \tag{5.5}$$

If, as suggested by figure 5, $\sigma_T(s) = \sigma(\text{total})$ tends to a constant value as $s \to \infty$, then for large s

$$\text{Im}\, F(s, 0) \sim s(\text{constant}). \tag{5.6}$$

Comparing equation (5.4) and (5.6) we see that

$$\alpha_0^+(t = 0) = 1. \tag{5.7}$$

This establishes that, in order to obtain an asymptotically constant total cross section, there must be a trajectory that goes through 1 at $t = 0$. The signature must be even (an odd-signature term of power s from (5.3) has zero imaginary part). This even-signature trajectory is called the Pomeranchuk trajectory and denoted α_P, thus

$$\alpha_P(t = 0) = 1. \tag{5.8}$$

Since the signature is even, there is no corresponding physical particle at $t = 0$, but the trajectory could correspond to a physical particle at $\alpha_P = 2$. The slope α_P' of this trajectory is rather uncertain (see equation (5.19) and figure 26) and no corresponding particle at $\alpha_P = 2$ has been uniquely identified. The object that is exchanged and gives rise to $\alpha_P(t)$ is called the Pomeron, or Pomeranchukon. The above conclusion remains valid also when the elastically scattered particles have nonzero spin, for example, in πN scattering.

5.3. *Total cross sections and leading Regge trajectories*

Exchanged 'Reggeons' (Regge trajectories) must satisfy conservation laws appropriate to the crossed channel. Elastic scattering in the s channel always allows the exchange of vacuum quantum numbers in the t channel. The Pomeron P, noted in the previous section, is one example of a trajectory of even signature and carrying only the quantum numbers of the vacuum (zero charge, zero strangeness, etc).

The leading correction terms to Pomeron exchange in π^+p and π^-p elastic scattering come from exchange of a Reggeon P' having the same quantum numbers as P, and from exchange of the ρ trajectory. Symbolically, using the optical theorem, one can write

$$s\sigma_T(\pi^- \text{p}) \sim P + P' + \rho \tag{5.9}$$

$$s\sigma_T(\pi^+ \text{p}) \sim P + P' - \rho \tag{5.10}$$

where P denotes $\text{Im}\, F(s, 0)$ given by equation (5.4) and P' and ρ denote similar expressions but with smaller values of $\alpha_n(0)$. Thus (5.9) and (5.10) have the form

$$\sigma_T(\pi^- \text{p}) \sim c_0 s^{(\alpha_0 - 1)} + c_1 s^{(\alpha_1 - 1)} + c_2 s^{(\alpha_2 - 1)} \tag{5.11}$$

$$\sigma_T(\pi^+ \text{p}) \sim c_0 s^{(\alpha_0 - 1)} + c_1 s^{(\alpha_1 - 1)} - c_2 s^{(\alpha_2 - 1)} \tag{5.12}$$

where

$$\alpha_0 = \alpha_P(0) = 1 \qquad \alpha_1 = \alpha_{P'}(0) \qquad \alpha_2 = \alpha_\rho(0).$$

The values of the constants in (5.11) and (5.12) can in principle be obtained from the experimental points in figure 5. It is found that only a poor fit is obtained if $c_1 = 0$; for this reason it is believed that there must be a Regge trajectory P', although it may be a pole approximating a branch cut rather than a genuine Regge pole.

The difference of (5.11) and (5.12) gives

$$\ln\{\sigma_T(\pi^- p)-\sigma_T(\pi^+ p)\}\sim \ln(2c_2)+(\alpha_2-1)\ln(s). \tag{5.13}$$

According to the experimental results shown in figure 6, and noted after equation (2.2),

$$2c_2\simeq 4 \text{ mb} \qquad (\alpha_2-1)\simeq -0{\cdot}31\pm 0{\cdot}04 \tag{5.14}$$

This gives $\alpha_\rho(0)=\alpha_2\simeq 0{\cdot}69\pm 0{\cdot}04$. Such a value is unexpectedly high and it is not consistent with the ρ trajectory illustrated in figure 21(b). It seems likely that (5.9) and (5.10) oversimplify the situation and more trajectories should be taken into account. This would lead to a more complicated form for $\Delta\sigma(\pi p)$, such as that in equation (2.3) for example.

Other total cross sections that can be studied in a similar manner are those for $\bar{p}p$ and pp collisions and for $K^- p$ and $K^+ p$ collisions. Each of these is thought to involve at least five Reggeons (P, P', ρ, ω, A_2). However, the increase of $\sigma_T(K^+ p)$ indicated in figure 5 is difficult to explain without also including at least one Regge branch cut (Frautschi and Margolis 1968, Barger and Phillips 1969, 1970, Phillips 1971).

5.4. *Phase-energy relations*

The phase of the amplitude (5.3) is determined from the same parameters as are shown in (5.11) and (5.12). The latter involve only $\operatorname{Im}F(s,0)$ but each term, F_n say, in (5.3) has $\operatorname{Re}F/\operatorname{Im}F$ equal to $\cot\pi(1-\frac{1}{2}\alpha)$ for even signature, and $-\tan\pi(1-\frac{1}{2}\alpha)$ for odd signature. Hence if we assume only P, P', ρ exchange in πp scattering, (5.3) and (5.11) give the ratio $\operatorname{Re}F(s,0)/\operatorname{Im}F(s,0)$ for forward $\pi^- p$ scattering in terms of the constants shown in (5.11). Similarly, (5.12) leads to the corresponding ratio for $\pi^+ p$ elastic scattering.

The phases of the forward $\pi^- p$ and $\pi^+ p$ scattering amplitudes have been measured (Foley *et al* 1967). They agree qualitatively with the total cross-section data, but they are not yet precise enough to give a detailed check on the parameters.

5.5. *The forward elastic peak*

For simplicity we will consider energies sufficiently high so that only the Pomeron pole need be considered. Then a scattering amplitude would take the form

$$F(s,t)\sim b_0(t)\exp\{\alpha_0(t)\ln(s)\}. \tag{5.15}$$

Assuming that near $t=0$, the Pomeron trajectory has slope α', we obtain

$$\alpha_0(t)=1+\alpha' t+\ldots. \tag{5.16}$$

Then, from equation (1.30) the differential cross section, near $t=0$ as $s\to\infty$, will have the form

$$\frac{d\sigma}{dt}\sim\frac{|b_0|^2}{16\pi}\exp\{2\alpha' t\ln(s)\}. \tag{5.17}$$

In the physical region t is negative. This result therefore predicts that the forward elastic peak has a width $\Delta(s)$ (at relative height $1/e$),

$$\Delta(s)\sim\frac{1}{2\alpha'\ln(s)}. \tag{5.18}$$

Experimental confirmation of the formula (5.17) is shown in figure 26, where $b(s)$ is plotted against $p(\text{lab}) \sim \frac{1}{2}s$ on a log scale. The quantity $b(s)$ is obtained by fitting experimental values of differential cross sections to the formula

$$\frac{d\sigma}{dt} = \left(\frac{d\sigma}{dt}\right)_{t=0} \exp\{2tb(s)\}. \tag{5.19}$$

The best linear fit to the high-energy data shown in figure 26 for proton–proton scattering gives

$$b(s) \simeq 0{\cdot}4 \ln(s). \tag{5.20}$$

Thus the slope of the Pomeron trajectory, α' in equation (5.17) appears to be 0·4, which is considerably less than the value of 1·0 that was indicated by the Regge trajectories shown in figure 21. There are various ways to explain this discrepancy;

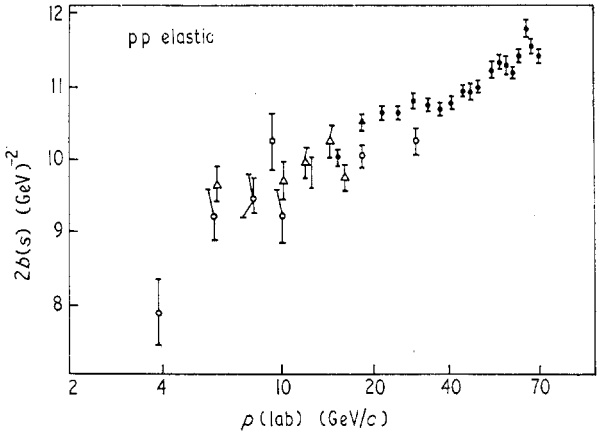

Figure 26. Experimental values for the slope $2b(s)$ of the elastic forward peak in the differential cross section for proton–proton scattering.

one possibility is that the Pomeron trajectory is exceptional (because it is the leading trajectory) so it could have a different slope from all others. Another possibility is that the data in figure 26 are not sufficiently asymptotic and $F(s, t)$ cannot be approximated by a single term as in equation (5.15), but more terms are significant. The latter possibility is strengthened by data on $b(s)$ (equation (5.19)) from other processes, for example in K^-p scattering $b(s)$ is nearly constant up to the region of 20 GeV/c laboratory momentum.

5.6. *The effects of particle spin, πN scattering*

Experimental results for π^-p charge-exchange scattering are illustrated in figure 13. There is a flattening of the differential cross section in the forward direction ($t = 0$), which becomes a dip at the higher energies. Such a dip cannot be explained by a single amplitude in a Regge pole model, since this gives a form like that in equation (5.19).

If allowance is made for nucleon spin, the π^-p exchange amplitude contains a 'spin non-flip' amplitude $f(s, t)$ and a 'spin-flip' amplitude $g(s, t)$. The latter vanishes in the forward direction. The former cannot vanish, since it is related to the total cross section difference $\sigma_T(\pi^-p) - \sigma_T(\pi^+p)$ by isospin invariance.

The differential cross section has the form (assuming only ρ exchange)

$$\frac{d\sigma(\pi^- p \to \pi^0 n)}{dt} \sim \frac{s^{2\alpha_\rho - 2}\eta_\pi^2(\eta_N^2 + \phi_N^2)}{\cos^2(\pi\alpha_\rho/2)} \tag{5.21}$$

where $\alpha_\rho = \alpha_\rho(t)$ is the ρ trajectory, η_π denotes coupling of ρ to π, and η_N the non-spin-flip coupling to the nucleon. The spin-flip coupling ϕ_N vanishes at $t = 0$. Thus the experimental results shown in figure 13 show that ϕ_N is large except at $t = 0$.

It is often assumed in Regge models that the residues, like $\eta_\pi^2(\eta_N^2 + \phi_N^2)$ in (5.21), become zero at all values of t for which $\alpha_\rho(t)$ is a negative integer or zero. This not only prevents an unphysical infinitity in (5.21) at negative odd integers, but it also introduces zeros in the leading term (shown in (5.21)) when $\alpha_\rho = 0, -2, -4 \ldots$. The first of these zeros, according to the trajectory for $\alpha_\rho(t)$ shown in figure 21, should be at $t = -0{\cdot}5$. This approximates closely to the dip that appears in the experimental results in figure 13.

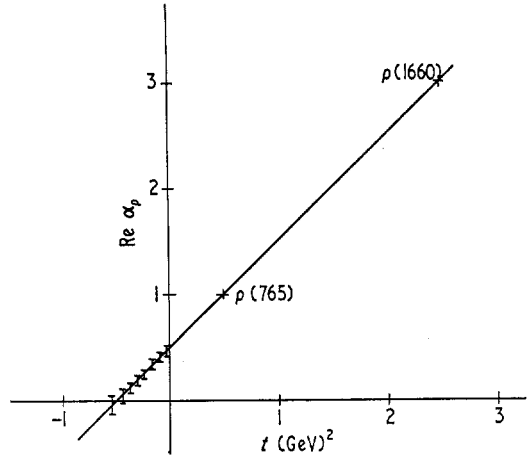

Figure 27. The ρ trajectory $\alpha_\rho(t)$ evaluated for $t < 0$ from data on πN charge exchange scattering (Ter Matirosyan 1966).

Using the experimental results of figure 13 and the formula (5.21) it is possible to evaluate $\alpha_\rho(t)$ for $t < 0$. The resulting values are shown in figure 27 and are in good agreement with the ρ trajectory illustrated in figure 21. However, it should be noted that agreement with figure 13 can also be obtained by using a Regge cut as well as the ρ pole but not assuming zeros of η and ϕ in (5.21) at $t = -0{\cdot}5$ (Kane *et al* 1969, 1970).

5.7. *Polarization*

It was noted in equation (3.24) that the polarization $P(\theta)$ in πN scattering is given by

$$P(s, t) = 2\,\mathrm{Im}\,(f^* g) \tag{5.22}$$

where $f = f(s, t)$ is the non-spin-flip amplitude and $g = g(s, t)$ is the spin-flip amplitude.

If only one Reggeon contributes to the $\pi^- p$ to $\pi^0 n$ scattering amplitude, the phase is determined as in equation (4.42) for a single odd signature term. Further, it has generally been assumed in Regge theory that such a Reggeon couples equally for spin-flip and non-spin-flip so that f and g would have the same phase. Then the polarization given by equation (5.22) would be zero.

Experimentally it is found that the polarization $P(s, t)$ for $\pi^- p$ charge exchange remains fairly constant up to 16 GeV/c at a value 10 to 15%, for t out to about 0·3 GeV^2. This confirms the suggestion made earlier, that there is at least one more Reggeon making significant contributions to the process $\pi^- p \to \pi^0 n$. Additionally, it could be that f and g are differently coupled to Reggeons.

5.8. *Fermion Regge poles and backward scattering*

In $\pi^+ p$ backward scattering, neutron exchange is allowed as shown in figure 28(*a*), and N*^{0}(1236) exchange can also take place (figure 28(*b*)). However, in $\pi^- p$ backward scattering neutron or proton exchange is forbidden by charge

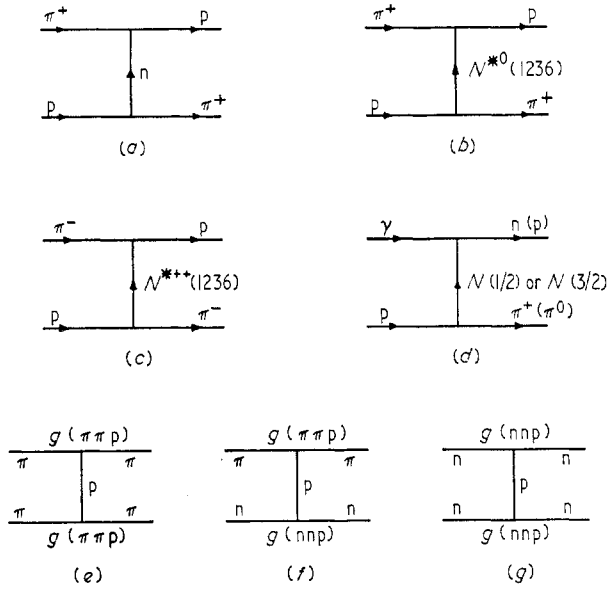

Figure 28. (*a*)–(*d*) show baryon exchange diagrams related to the backward scattering discussed in §§ 5.8 and 5.9. (*e*)–(*g*) illustrate the factorization of Regge residues discussed in § 5.10.

conservation, but N*++(1236) exchange is allowed (figure 28(*c*)). If we assume that near to backward scattering, the amplitudes are dominated by the Reggeons corresponding to the allowed exchanges, the differences between $\pi^+ p$ and $\pi^- p$ may be attributed to the effect of neutron Regge exchange.

Fermion Regge poles create nontrivial complications in the Regge formalism, not only in the spin-coupling coefficients, but also because they are liable to introduce spurious singularities. The latter have to be cancelled somehow, for consistency, but there is some ambiguity in how to do it. We will not enter into these complications here; they are outlined in the book by Collins and Squires (1968) and in the review by Collins (1971) who lists further references.

The differential cross section at fixed u takes the form

$$\frac{d\sigma}{du} \sim \frac{1}{64\pi^2 ks^{1/2}} \left\{ \left| \beta^+ \left(\frac{1+\exp(-i\pi)(\alpha^+ - \frac{1}{2})}{\cos \pi\alpha^+} \right) \left(\frac{s}{s_0} \right)^{\alpha^+ - \frac{1}{2}} \right|^2 + \left| \beta^- \left(\frac{1+\exp(-i\pi)(\alpha^- - \frac{1}{2})}{\cos \pi\alpha^-} \right) \left(\frac{s}{s_0} \right)^{\alpha^- - \frac{1}{2}} \right|^2 \right\} \tag{5.23}$$

where $\alpha^+(\sqrt{u})$ and $\alpha^-(\sqrt{u})$ correspond to natural and unnatural parity Regge trajectories. They satisfy a symmetry relation

$$\alpha^+(\sqrt{u}) = \alpha^-(\sqrt{-u}) \tag{5.24}$$

and there is also a relation between the residues β^+ and β^-.

The residues β^+ and β^- in (5.23) are required to have zeros to kill unphysical divergences due to zeros of $\cos \pi\alpha^\pm$. They are often assumed, therefore, to have zeros for

$$\alpha^+ = -\tfrac{1}{2}, -\tfrac{3}{2}, \ldots \qquad \alpha^- = -\tfrac{1}{2}, -\tfrac{3}{2}, \ldots . \tag{5.25}$$

Then the phase factors in (5.23) will produce zeros in the terms shown (the leading terms by assumption). The zero in the neutron exchange term can be estimated from the trajectory shown in figure 21(*a*). This gives

$$\alpha_N(u) = -\tfrac{1}{2} \quad \text{at} \quad u = -0{\cdot}2 \text{ GeV}^2. \tag{5.26}$$

Hence we have a preliminary interpretation of the dip in $\pi^+ p$ scattering at $u = -0{\cdot}2$, shown in figure 14. Neutron Regge exchange is not permitted in $\pi^- p$ scattering and no dip is observed. Both $\pi^+ p$ and $\pi^- p$ have N*(1236) exchange and this may contribute a large part of $\pi^- p$ scattering near $u = 0$. Alternative explanations of the dip in $\pi^+ p$ scattering may be obtained by means of Regge cuts using pole-cut destructive interference (Kane *et al* 1969, 1970).

For suitably chosen processes in the backward direction there is no known Regge trajectory that can be exchanged. This situation occurs with

$$K^- p \to p K^- \tag{5.27}$$

The cross section for this process decreases like s^{-9} near $u = 0$ (but at relatively low values of $s \sim 3$ GeV^2). A double Regge exchange is possible (of K^+ and Δ). This would produce a Regge branch cut which would correspond to a backward cross section decreasing faster than s^{-3}.

5.9. *Photoproduction*

Photoproduction processes at high energies may be considered by means of Regge theory in a similar manner to two-body reactions involving only strong interactions. Thus the two processes

$$\gamma p \to n\pi^+ \qquad \gamma p \to p\pi^0 \tag{5.28}$$

in the near backward direction are related to $\pi^+ p$ or $\pi^- p$ scattering. Both of the processes (5.28) can involve N(938) or N*(1236) exchange (isospin $\frac{1}{2}$, or $\frac{3}{2}$ as shown in figure 28(*d*)). One might therefore expect a dip at $u \simeq -0{\cdot}2$, similar to that found for $\pi^+ p$. Such a dip has not been observed, indicating that the simplest Regge model described in § 5.8 above is not adequate.

5.10. *Two-body reactions in general*

In the previous sections we have shown in several examples how Regge pole models can give a simple preliminary fit to the data that is not valid when a wider range of experimental information is considered. This should not be taken as a sign of failure of Regge theory but rather as confirmation that it involves a non-trivial parametrization of collision amplitudes. If a Regge trajectory is allowed in two different reactions, there will be a relation between its contribution to the two reaction amplitudes. If this contribution vanishes for a certain value of t in one amplitude it may also vanish in the other.

The relation between Regge poles and resonance poles suggests strongly that residues at poles factorize in the manner illustrated in figure 28(*e*)(*f*)(*g*). This indicates that the residues at the Pomeron pole are products of the coupling constants g that are shown in the diagrams. Thus for $\pi\pi$ scattering (5.4) would become

$$F_{\pi\pi}(s, 0) \sim \mathrm{i}(g(\pi\pi\mathrm{P}))^2\left(\frac{s}{s_0}\right). \tag{5.29}$$

Similarly πN and NN scattering would give

$$F_{\pi\mathrm{N}} \sim \mathrm{i}g(\pi\pi\mathrm{P})\, g(\mathrm{NNP})\left(\frac{s}{s_0}\right) \tag{5.30}$$

$$F_{\mathrm{NN}} \sim \mathrm{i}(g(\mathrm{NNP}))^2\left(\frac{s}{s_0}\right). \tag{5.31}$$

Using the optical theorem this gives

$$\sigma_{\mathrm{T}}(\pi\pi)\,\sigma_{\mathrm{T}}(\mathrm{NN}) \sim \sigma_{\mathrm{T}}(\pi\mathrm{N})^2. \tag{5.32}$$

Although this relation is not directly measurable, it shows that factorization provides a powerful restriction on results from Regge theory. It gives relations between Regge pole contributions that occur in different two-body reactions. This severely reduces the number of parameters that are available for fitting data. Although the number of parameters may be large, when one takes into account spin complications and correction terms due to nonleading Regge trajectories or branch cuts, there will be a very large amount of experimental data available when a detailed study has been made of all possible reactions resulting in the particles or resonances that were listed in table 1. We will not give an exhaustive list of these reactions (an extensive, but still incomplete, list by Collins (1971) shows more than seventy five two-body or quasi-two-body reactions). Instead we will give some illustrative examples of different types of reaction and show the leading Regge trajectories in each case. They are classified according to the type of Reggeon exchange that is expected to dominate at high energies. The Reggeons are denoted by the leading particle (resonance) on each trajectory.

Charge exchange (near forward)

$\pi^-\mathrm{p} \to \pi^0\mathrm{n}$ (ρ exchange)

$\pi^-\mathrm{p} \to \omega^0\mathrm{n}$ (ρ)

$\mathrm{K}^-\mathrm{p} \to \bar{\mathrm{K}}^0\mathrm{n}$ ($\rho + A_2$)

$\gamma\mathrm{p} \to \pi^0\mathrm{p}$ ($\rho + \omega$)

The baryons on the right-hand side of these reactions could involve resonances instead of n or p. Similarly, baryons in reactions listed below could be replaced by resonances.

Strangeness exchange (*near forward*)

$$\pi^- p \to K^0 \Lambda \qquad (K(494) + K(892))$$
$$K^- p \to \pi^- \Sigma^+ \qquad (K(494) + K(892))$$

Pseudoscalar meson exchange (*near forward*)

$$\pi^- p \to A_2^0 n \qquad (\pi \text{ exchange})$$
$$\pi^- p \to \rho^0 \Delta(1236) \qquad (\pi + A_2)$$
$$\pi^- p \to \rho^0 n \qquad (\pi + \omega + A_2)$$
$$pn \to np \qquad (\pi + \rho + \omega + A_2)$$
$$\gamma p \to \pi^- \Delta^{++}(1236) \qquad (\pi + \rho + A_2)$$

Baryon exchange (*near backward*)

$$\pi^- p \to \pi^- p \qquad (\Delta(1236))$$
$$\pi^+ p \to \pi^+ p \qquad (N(938) + \Delta(1236)$$
$$\gamma p \to \pi^+ n \qquad (N(938) + \Delta(1236)$$

Elastic scattering (*near forward*)

$$\pi^- p \to \pi^- p \qquad (P + P' + \rho)$$
$$K^- p \to K^- p \qquad (P + P' + \rho + \omega + A_2)$$
$$K^+ p \to K^+ p \qquad (P + P' - \rho - \omega + A_2)$$

Quasi-elastic (*near forward*)

$$\pi p \to \pi N^+(1400) \qquad (P + P' + \rho)$$
$$\gamma p \to \rho^0 p \qquad (P + P' + A_2 + \pi)$$

Exotic exchange (*near forward*)

No known single Reggeon exchange is allowed but double Reggeon (branch cut) exchange can take place.

$$\pi^- p \to K^+ \Sigma^- \qquad (\rho K(892) \text{ cut})$$
$$\pi^- p \to \pi^+ \Delta^-(1236) \qquad (\rho\rho \text{ cut})$$

Exotic baryon exchange (*near backward*)

$$K^- p \to K^- p \qquad (K(892)\,\Delta(1236) \text{ cut})$$
$$\bar{p} p \to \Lambda \bar{\Lambda} \qquad (N\Lambda \text{ cut})$$

We conclude this section by noting again that (i) the above list shows only a selection of reactions and (ii) there may be significant contributions from Reggeon exchange, either of poles or cuts, other than those listed as the leading trajectories.

6. Developments from Regge theory—duality

In this section several developments from Regge theory will be outlined. The first of these is an attempt to combine information about low-energy collisions with high-energy Regge theory, which leads to 'finite energy sum rules'. The second concerns an apparent (approximate) equivalence of Regge theory to an average over resonances at low energies, for certain scattering amplitudes. This equivalence is called 'duality', and is explicitly shown in a representation due to Veneziano, which forms the third topic in this section. We will conclude with a brief discussion of some aspects of Regge theory applied to many-particle production in high-energy collisions.

6.1. *Finite energy sum rules*

These rules will be denoted by FESR in the following discussion. They were first used by Igi (1962, 1963) when he deduced that a second trajectory, the P', was necessary for fitting πN data, in addition to the Pomeron trajectory and others

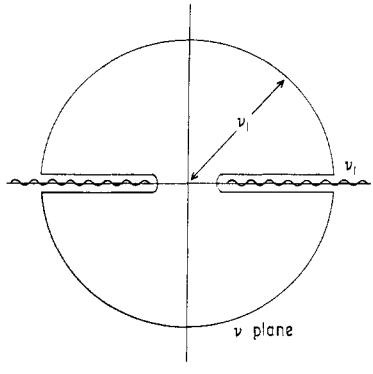

Figure 29. The contour in the complex ν plane used in deriving the FESR given in equation (6.6).

associated with mesons. However, their significance as a starting point for a discussion of duality was not noticed until much later, when they were developed independently by several groups, including Logunov *et al* (1967), Igi and Matsuda (1967a, b) and Dolen *et al* (1967, 1968).

The general idea of FESR is to use a dispersion relation at fixed momentum transfer (fixed t) and approximate the high-energy part of the integral by several Regge poles. The simplest derivation is by means of Cauchy's theorem using the contour shown in figure 29, where the variable ν is defined by

$$\nu = \frac{s-u}{4m}. \tag{6.1}$$

For illustration, we consider a scattering amplitude $F(\nu, t)$ having no bound-state poles and antisymmetric under $\nu \to -\nu$. Then, integrating $F(\nu, t)$ round the closed contour shown in figure 29, gives zero. Hence

$$\int_{-\nu_1}^{0} d\nu\{F(\nu+i\epsilon)-F(\nu-i\epsilon)\}+\int_{0}^{\nu_1} d\nu\{F(\nu+i\epsilon)-F(\nu-i\epsilon)\} = -\int_C d\nu\, F(\nu) \tag{6.2}$$

where C denotes the circular part of the contour $|\nu| = \nu_1$. From the antisymmetry

of F, the left-hand side of (6.2) gives

$$4\mathrm{i}\int_0^{\nu_1}\mathrm{d}\nu\,\mathrm{Im}\,F(\nu,t). \tag{6.3}$$

The right-hand side of (6.2) is now approximated by the Regge pole form for an antisymmetric amplitude given in equation (5.3) (odd signature),

$$F(\nu)\simeq\sum_n\beta_n(t)\,\nu^{\alpha_n}\{\mathrm{i}+\tan(\tfrac{1}{2}\pi\alpha_n)\}. \tag{6.4}$$

With this approximation, after using the antisymmetry of $F(\nu)$, one obtains

$$-\int_C\mathrm{d}\nu\,F(\nu)\simeq-2\sum_n\beta_n\,\nu_1^{\alpha_n+1}\int_0^{\pi}\mathrm{i}\,\mathrm{d}\theta\exp[\mathrm{i}\theta(\alpha_n+1)](\mathrm{i}+\tan\tfrac{1}{2}\pi\alpha_n)$$

$$\simeq 4\mathrm{i}\sum_n\beta_n\,\nu_1^{\alpha_n+1}\left(\frac{1}{\alpha_n+1}\right). \tag{6.5}$$

From (6.3) and (6.5) one obtains the FESR

$$\int_0^{\nu_1}\mathrm{d}\nu\,\mathrm{Im}\,F(\nu,t)\simeq\sum_n\frac{\beta_n\,\nu_1^{\alpha_n+1}}{\alpha_n+1}. \tag{6.6}$$

More generally, whether $F(\nu,t)$ is symmetric or antisymmetric, one can choose N so that $\nu^N F(\nu,t)$ is antisymmetric in ν. One then obtains the FESR,

$$\int_0^{\nu_1}\mathrm{d}\nu\,\nu^N\,\mathrm{Im}\,F(\nu,t)\simeq\sum_n\frac{\beta_n\,\nu_1^{\alpha_n+N+1}}{\alpha_n+N+1}. \tag{6.7}$$

If $F(\nu,t)$ has bound-state poles, there will be additional terms containing their residues.

FESR provide additional constraints on Regge parameters in that they demand consistency with low-energy data as well as high-energy data, although the Regge content of FESR occurs only at high energies. An excellent review of applications of FESR has been given by Jackson (1969), who gives further references. We will note one particular application in the next section.

6.2. *Duality and exchange degeneracy*

The FESR (6.6) may be applied to the antisymmetric pion–nucleon forward scattering amplitude, $A^{(-)}+\nu B^{(-)}$ at $t=0$. Then, by the optical theorem, the left-hand side can be expressed as an integral involving differences of $\pi^-\mathrm{p}$ and $\pi^+\mathrm{p}$ total cross sections. The right-hand side should involve only the ρ meson Regge trajectory. Each side can therefore be plotted as a function of ν_1, the left-hand side being given by experiment, the right-hand side by Regge theory. A comparison made by Igi and Matsuda (1967a) is shown in figure 30.

The two curves in figure 30 suggest the possibility that in the low-energy region the Regge amplitude may represent an average amplitude in which the local fluctuations due to resonance are smoothed out in some suitably chosen manner. It will be recalled that the Regge amplitude was obtained from resonances in the t channel. The idea suggested by figure 30 is that the Regge amplitude may also be regarded as an average over resonances in the s channel. This idea has been given the name 'duality'.

It should be emphasized that duality is an idea rather than a theory. It has many different interpretations, some of which we will illustrate here, but it does not lead to unique prescriptions. Its simplest form, illustrated in figure 30, receives considerable support from the FESR for the same amplitude at values of t not equal to zero (Dolen *et al* 1968). It was noted (following equation (5.21)) that there is evidence for a zero in the ρ trajectory's residue $\beta(t)$ at $t \simeq -0{\cdot}5$. Since, only the ρ trajectory contributes to the FESR for the antisymmetric πN amplitude, the right-hand side of equation (6.6) should be zero at $t \simeq -0{\cdot}5$. The left-hand side (for $t < 0$) can be obtained from phase-shift solutions in the low-energy region and it is found to have a pronounced minimum near $t = -0{\cdot}5$.

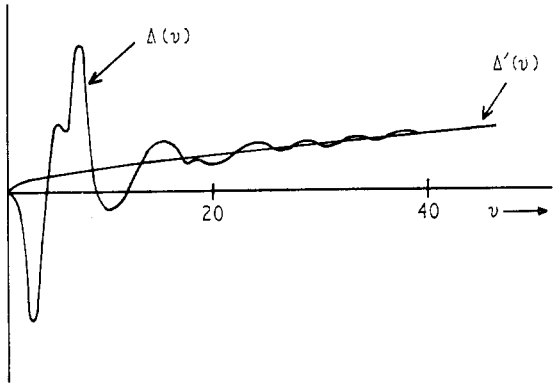

Figure 30. The left-hand side of the FESR equation (6.6) is denoted Δ for an antisymmetric πN forward amplitude. The right-hand side is denoted Δ', derived from ρ Regge exchange. Both are plotted against ν defined in equation (6.1) (from Igi and Matsuda 1967a). (ν is measured in units of the pion mass, and the units of Δ, Δ' are arbitrary.)

Another aspect of duality was noticed by Schmid (1968). He observed that the partial wave amplitudes obtained from the Regge amplitude corresponding to single ρ exchange have a resonance-like behaviour. The partial wave phase-shifts go through $\frac{1}{2}\pi$, sometimes at a sequence of energy values that approximates to a sequence of resonances. This remark like those about FESR and duality applies only to certain amplitudes. In particular, those amplitudes (eg elastic amplitudes) that involve Pomeron exchange do not satisfy either aspect of duality.

A third aspect of duality may be illustrated by K^+p scattering and K^-p scattering. The former has no resonances, and therefore should have a small cross section if the Pomeron (non-dual) part of the amplitude is excluded. We have, in fact, contributions to K^+p and K^-p scattering from P, P', ω, A_2 and ρ,

$$F(K^-p) = P + P' + \omega + A_2 + \rho \tag{6.8}$$

$$F(K^+p) = P + P' - \omega + A_2 - \rho. \tag{6.9}$$

Thus, if we accept that the Pomeron is non-dual, then the remainder of the K^+p amplitude should be small. This can be achieved if we have equality between the Regge contributions, namely,

$$P' \equiv \omega \quad \text{and} \quad A_2 \equiv \rho. \tag{6.10}$$

The P' is an even signature trajectory, whereas the ω is odd signature. Equation (6.10) states that both Regge trajectories are the same and that their residues are

also the same. This is precisely the situation that occurred in our simple illustration of Regge theory in § 4.4. It occurs in potential scattering when there are no exchange forces. In relativistic theory the equivalence of a pair of odd and even signature Regge trajectories (and their residues) is described as 'exchange degeneracy'. Note that exchange degeneracy is only approximate. It implies that only the Pomeron contributes to K^+p scattering, but owing to the sign differences between (6.8) and (6.9) both the P', ω and the A_2, ρ trajectories contribute to K^-p scattering.

We have noted above that duality implies an equivalence between Regge amplitudes and suitably averaged resonance amplitudes. However, the contribution from the Pomeron Regge trajectory is exceptional and (if present) it must be subtracted in order to obtain the equivalence implied by duality. A method for expressing duality in mathematical form will be described in the next section.

6.3. *The Veneziano representation*

Duality requires subtraction of any Pomeron contribution that occurs in a scattering amplitude. Although this contribution is quite well defined at high energies, it is somewhat uncertain at low energies. One can therefore obtain the clearest statement of duality by considering the reaction which was used in his basic paper by Veneziano (1968), namely,

$$\pi\pi \to \pi\omega. \tag{6.11}$$

This reaction has isospin one, as does each crossed reaction. Therefore, there is no Pomeron contribution in any of the three channels. Furthermore, after factorizing out a kinematic factor there is just one scalar amplitude $A(s, t)$, which is a function of the invariants s and t or of u related to s and t by

$$s + t + u = 4m^2. \tag{6.12}$$

For simplicity we take the π and ω (and later the ρ) to have equal masses m.

The three channels, in which s, t and u, respectively, denote the energy squared are all the same as (6.11). To be specific, we include the charge;

$$s \text{ channel}, \quad \pi^+\pi^0 \to \pi^+\omega \tag{6.13a}$$

$$t \text{ channel}, \quad \pi^+\pi^- \to \pi^0\omega \tag{6.13b}$$

$$u \text{ channel}, \quad \pi^+\omega \to \pi^+\pi^0. \tag{6.13c}$$

The kinematics and crossing properties from one channel to another were described in § 3.1 and in figure 19.

In each of the three channels, the ρ meson represents an intermediate state or resonance. The associated sequence of resonances on the ρ Regge trajectory are therefore symmetrically present in each channel. For the present though, we will proceed unsymmetrically, and initially we will ignore the resonances in the u channel. Then we can concentrate on obtaining duality between the s and t channels. At a later stage we will symmetrize to include also the u channel.

We will consider only the ρ sequence of resonances for simplicity. Therefore in the s channel the amplitude should be expressible in terms of a sum over these successive resonances.

$$A(s, t) = \sum_n \frac{r}{s - s_n} \tag{6.14}$$

where $s_n = m_n^2$ and m_n is the mass of the nth resonance on the ρ Regge trajectory, thus $n = 0$ gives the ρ meson and

$$\alpha(m_n^2) = 2n+1. \tag{6.15}$$

We make the usual linear approximation for the trajectory and take $\epsilon(s)$ to be small in

$$\alpha(s) \simeq \alpha_0 + s + i\epsilon(s). \tag{6.16}$$

At high energies, the amplitude will be dominated by the Regge pole exchange in the t channel, which is also the ρ meson, thus as $s \to \infty$,

$$A(s,t) \sim \beta(t)\, s^{\alpha(t)-1}. \tag{6.17}$$

The value $\alpha(t)-1$ replaces the usual $\alpha(t)$ in the asymptotic Regge form because we have removed a kinematic factor which is due to the spin of the ω meson and which has an asymptotic behaviour proportional to s.

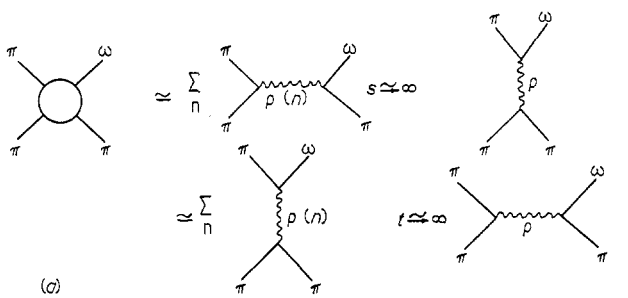

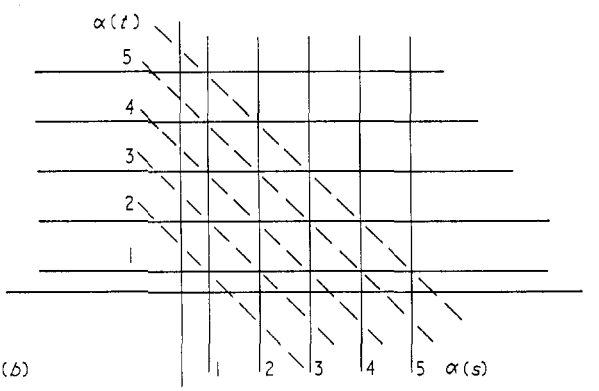

Figure 31. (*a*) Schematic approximations illustrating duality between resonances and Regge behaviour. (*b*) $\alpha(s)$, $\alpha(t)$ diagram showing poles of the Veneziano form of Euler's beta function (6.19). Zeros are denoted by the broken lines, poles by the continuous lines at integer values of $\alpha(s)$ and $\alpha(t)$.

The idea of duality shown schematically in figure 31(*a*) asserts that (6.17) is simply the asymptotic form of the sum over resonances (6.14). Veneziano (1968) made the important observation that the Euler beta function has the desired property of giving both the forms (6.14) and (6.17) and also can be written symmetrically

in s and t. He therefore took as a trial scattering amplitude

$$A(s,t) = B(1-\alpha(s), 1-\alpha(t)) \tag{6.18}$$

$$= \frac{\Gamma(1-\alpha(s))\,\Gamma(1-\alpha(t))}{\Gamma(2-\alpha(s)-\alpha(t))}. \tag{6.19}$$

We have omitted an arbitrary normalization constant. This function has poles at fixed s and at fixed t,

$$1-\alpha(s) = -n \qquad 1-\alpha(t) = -m \tag{6.20}$$

for m, $n = 0, 1, 2, \ldots$. It also has lines of zeros, due to the poles in the Γ function in the denominator, when

$$2-\alpha(s)-\alpha(t) = -l \qquad (l = 0, 1, 2, \ldots). \tag{6.21}$$

These poles and zeros are illustrated in figure 31(b). Thus the beta function (6.19) has

(i) poles in the s and t channels, corresponding to an exchange degenerate ρ trajectory,
(ii) symmetry between s and t,
(iii) no double poles.

The absence of double poles follows from the fact that the zeros shown in figure 31(b) meet the poles at their intersecting points.

The asymptotic behaviour of (6.19) for fixed t as $s \to \infty$ may be found from Stirling's formula

$$\Gamma(x) \sim (2\pi)^{1/2}\, \mathrm{e}^{-x}\, x^{x-\frac{1}{2}}. \tag{6.22}$$

This gives from (6.19), as $s \to \infty$,

$$A(s,t) \sim \frac{\pi(\alpha(s))^{\alpha(t)-1} \exp(-\mathrm{i}\pi\alpha(t)) \exp(1-\alpha(t))}{\Gamma(\alpha(t)) \sin(\pi\alpha(t))}. \tag{6.23}$$

This will have the Regge form (6.17), provided $\alpha(s)$ is a linear function of s, which is exactly the assumption (6.16). Then as $s \to \infty$,

$$A(s,t) \sim \frac{\pi s^{\alpha(t)-1} \exp(-\mathrm{i}\pi\alpha(t)) \exp(1-\alpha(t))}{\Gamma(\alpha(t)) \sin(\pi\alpha(t))}. \tag{6.24}$$

Since $\alpha(t)$ has a form similar to (6.16), we obtain for the Veneziano amplitude (6.19) the following result (iv).

(iv) Regge behaviour as $s \to \infty$ for fixed t, and as $t \to \infty$ for fixed s.

We have now achieved symmetry and duality between the s and t channels. This can be extended to give the s, t, u symmetry required for the reaction (6.11) by taking

$$A(s,t) = B(1-\alpha(s), 1-\alpha(t)) + B(1-\alpha(t), 1-\alpha(u)) + B(1-\alpha(u), 1-\alpha(s)). \tag{6.25}$$

There are of course a number of difficulties and deficiencies in this simplest form of Veneziano representation. Some are serious but others can be remedied. The principal defects that have not yet been adequately solved are:

(i) the amplitude is not unitary,
(ii) it is difficult to include spin one-half particles in the representation,
(iii) the amplitude is not unique in the sense that other beta functions can be added without spoiling the duality properties.

Advantages of the representation that have not been mentioned above include:

(i) convenient generalizations to multiparticle processes (Bardacki and Ruegg 1968, Virasoro 1969a, b).

(ii) applications give qualitative agreement with experimental results (Lovelace 1968, Chan 1969, Jacob 1970, Koba and Nielson 1969).

An example of an application of the Veneziano method is shown in figure 32, which compares theory (Lovelace 1968) and experiment (Anninos *et al* 1968) for the annihilation reaction

$$\bar{p}n \to \pi^+\pi^-\pi^-. \tag{6.26}$$

This reaction is viewed theoretically as the decay of an isovector meson ($\bar{p}n$) into three pairs. It may be represented by a term like (6.19). Other terms could be

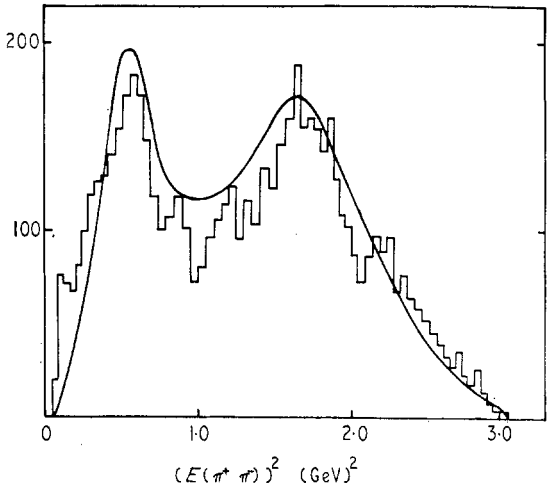

Figure 32. Comparison of the Veneziano model (6.19) (curved line) with the $\pi^+\pi^-$ mass (energy) distribution of experimental values, for the annihilation reaction, $\bar{p}n \to \pi^+\pi^-\pi^-$ (theoretical curve from Lovelace 1968, experimental values from Anninos *et al* 1968). The vertical axis denotes the number of events observed (in a small energy interval) at a given energy.

included, but it is found that this gives the reasonable agreement with experiment that is shown in figure 32. In making comparison with experiment, it is necessary to make some *ad hoc* allowance for unitarity by taking $\epsilon(s)$ in (6.16) to be nonzero. The form of $\alpha(s)$ used in (6.19) to give the curve shown in figure 32 is

$$\alpha(s) = 0{\cdot}48 + 0{\cdot}88s + i(0{\cdot}28)(s - 4\mu^2)^{1/2}. \tag{6.27}$$

Many other more complicated comparisons with experiment have been made. They yield good qualitative agreement, but it is not clear whether this is really significant in view of the fundamental defects noted above that necessitate *ad hoc* procedures when making comparison with experiment.

6.4. *Many-particle production*

At relatively low energies (a few GeV) the production of particles in a collision is strongly influenced by resonances between the produced particles. A simple application of Regge theory is precluded when the energies are in a resonance region.

We have already discussed in §§ 2.9 and 5.10 production processes which can be approximated as quasi-two-body reactions in which Regge theory becomes appropriate for sufficiently high incident energies. We have also indicated in § 6.3 that duality provides a method for extending Regge theory down into the resonance region by means of the Veneziano model and its extensions.

The applications of extensions of the Veneziano model (reviewed by Jacob 1970) have been concerned mainly with three-body production processes, although a major theoretical effort has been made to obtain a systematic treatment of many-body processes. The latter has not yet been successful, for the reasons noted in § 6.3, although some considerable progress has been made.

The study of many-body production processes at high energies (10 GeV to 2000 GeV) has not yet entered the stage of detailed comparison with experiment where the 'fine structure' of theory or experiment becomes crucial (as in two-body and quasi-two-body Regge theory). However, there have been extensive studies of experimental results based on four theoretical models, namely:

(i) A thermodynamic model (Hagedorn 1965, 1968, Hagedorn and Ranft 1968). This pictures the collision process as leading to a (momentum) distribution of decay centres (fireballs) which emit particles in a manner similar to black body radiation.

(ii) The multiperipheral model (Bertochi *et al* 1962, Amati *et al* 1962), which has a natural extension to a multi Regge model (Kibble 1963, Ter Matirosyan 1963, Polkinghorne 1965, Zachariasen and Zweig 1967, Zachariasen 1971, Chew and Pignotti 1968). We will briefly discuss this model below, it leads to some of the features of models (iii) and (iv) which are more intuitively based.

(iii) Feynman's parton model, in particular the scaling hypothesis in many-particle production at asymptotic energies (Feynman 1969).

(iv) The limiting fragmentation model of Yang and collaborators (Benecke *et al* 1969, Chou and Yang 1969) which suggests that the distribution of produced particles having finite momenta relative to the target (or the projectile) reaches a limiting form at asymptotically high energies.

In addition, one should mention the longitudinal phase-space picture suggested by Van Hove though this is primarily a method of analysis rather than a model (Van Hove 1969a,b). This picture and the other models for many-body production have been reviewed by Van Hove (1971) and by Horn (1972). The use of Regge theory and the multiperipheral model in many-body production has been reviewed by Jacob (1971).

The multiperipheral model assumes that a particle production process can be derived from a diagram like that illustrated in figure 33. This shows the incident particles with momenta p_1 and p_2 interacting via a chain of Regge exchanges $(k_1, k_2, \ldots)$ to produce final particles having momenta $q_1, q_2, \ldots, q_n$.

As we have seen in § 5.5, a Regge exchange leads to a forward peak in a two-particle reaction. The analogous argument applied to the multi-Regge exchange diagram in figure 33 leads to a strong preference towards small values for the exchanged momenta. This leads to small average values for the transverse momenta of the product particles in the final state, in agreement with the experimental results shown in figures 17 and 18. It also leads to small longitudinal momenta for produced particles (pions) associated with the central part of the chain in figure 33. It is not yet known whether this (pionization) phenomenon is in agreement with experiment.

The mean multiplicity of the produced number of particles can be evaluated from the multiperipheral model using an argument due to Fubini (1963) (see also Horn 1972). The n particle production cross section σ_n is given by the modulus squared of the amplitude corresponding to figure 33. Then, if g denotes the coupling constant,

$$\sigma_n = g^{2n} f(s, \ldots). \tag{6.28}$$

The total cross section is given by

$$\sigma_T = \sum_n \sigma_n. \tag{6.29}$$

The mean number of particles produced in the reaction is defined to be

$$\langle n \rangle = \frac{1}{\sigma_T} \sum n\sigma_n. \tag{6.30}$$

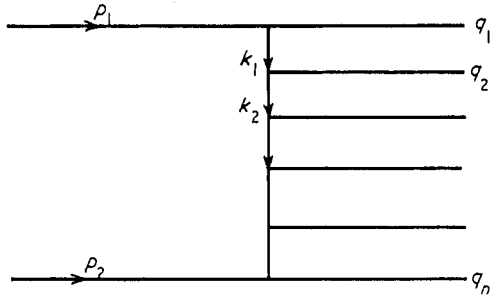

Figure 33. A schematic representation of a production process involving multi-Regge exchange that forms the basis for the multiperipheral model.

This can be derived by formally changing the coupling constant g^2 to λg^2. From (6.28) and (6.29) this gives the 'λ dependent' total cross section

$$\sigma_T(\lambda) = \sum \lambda^n \sigma_n. \tag{6.31}$$

Hence the average multiplicity (6.30) is given by

$$\langle n \rangle = \lim_{\lambda \to 1} \frac{\lambda}{\sigma_T(\lambda)} \left(\frac{\partial}{\partial \lambda} \sigma_T(\lambda) \right). \tag{6.32}$$

We now assume the result of Regge theory that σ_T is determined by the Pomeranchuk–Regge trajectory $\alpha(t)$ at $t = 0$. With $g^2 \to \lambda g^2$, $\alpha(t)$ at $t = 0$ will depend on λ, say $\alpha(\lambda)$. Then

$$\sigma_T(\lambda) = \beta(\lambda)\, s^{\alpha(\lambda)-1} \tag{6.33}$$

where the limit as $\lambda \to 1$ of $\alpha(\lambda)$ is 1. Using (6.32) and (6.33) we obtain

$$\langle n \rangle = a \ln(s) + b \tag{6.34}$$

where a and b are (unknown) constants. This result on the average multiplicity in a high-energy collision compares well with the experimental results in figure 34, which shows the average charged multiplicity. The latter has been verified (at machine energies up to 30 GeV) to be proportional to the total multiplicity.

A formula similar to (6.34) can also be derived from the models of Feynman and Yang *et al* which were mentioned above. The essential features of these models that lead to (6.34) can also be derived from the multiperipheral Regge model. It is possible that this result, like some other results in Regge theory, is due to certain

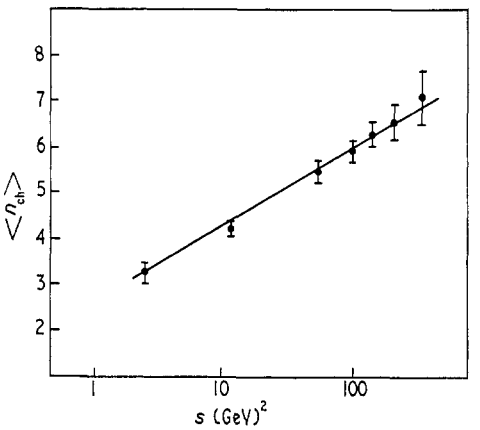

Figure 34. The average multiplicity of charged particles produced in pp collisions. The high-energy points are obtained from cosmic ray data (Jones *et al* 1970).

general features of the theory rather than the specific details of Regge models. If this is the case then a future task in both theory and experiment will be the identification and isolation of these general features. In the meantime Regge theory and its generalizations remain the most hopeful basis from which to develop a full understanding of the strong interactions of elementary particles.

Acknowledgments

Most of this review was written whilst the author was visiting the CERN high-energy physics laboratory in Geneva and the CNRS laboratory in Marseilles. The author wishes to thank Dr B Zumino of CERN and Dr A Visconti of CNRS for their hospitality and assistance. He also wishes to thank Miss Sue Mackenzie for typing the manuscript.

References

ALLABY J V 1970 *Proc. 15th Int. Conf. on High Energy Physics, Kiev* to be published
ALLABY J V *et al* 1968 *Phys. Lett.* **28B** 67
AMATI D *et al* 1962 *Nuovo Cim.* **26** 896
ANNINOS P *et al* 1968 *Phys. Rev. Lett.* **20** 402
BAKER W F *et al* 1968 *Phys. Lett.* **28B** 291
BARASH-SCHMIDT N *et al* 1971 *Rev. Mod. Phys.* **43** S1
BARDACKI K and RUEGG H 1968 *Phys. Lett.* **28B** 342
BARGER V and CLINE D 1969 *Phenomenological Theories of High Energy Scattering* (New York: Benjamin)
BARGER V and PHILLIPS R J N 1969 *Phys. Rev.* **187** 2210
—— 1970 *Phys. Lett.* **31** 643
BENECKE J *et al* 1969 *Phys. Rev.* **188** 2159
BERTOCHI L *et al* 1962 *Nuovo Cim.* **25** 626

BETHE H A 1958 *Ann. Phys. N.Y.* **3** 190
BLANKENBECLER R and GOLDBERGER M L 1962 *Phys. Rev.* **126** 766
CHAN, HONG MO 1969 *Phys. Lett.* **28B** 425
CHEW G F 1966 *The Analytic S Matrix* (New York: Benjamin)
CHEW G F and FRAUTSCHI S C 1961 *Phys. Rev. Lett.* **7** 394
—— 1962 *Phys. Rev. Lett.* **8** 41
CHEW G F, GELL-MANN M and ROSENFELD A H 1964 *Scient. Am.* **210** No 2 74
CHEW G F and PIGNOTTI A 1968 *Phys. Rev.* **176** 2112
CHOU T T and YANG C N 1969 *Phys. Rev. Lett.* **25** 1072
COLLINS P D P 1971 *Phys. Rep.* **1** 103
COLLINS P D P and SQUIRES E J 1968 *Regge Poles in Particle Physics* (Berlin: Springer-Verlag).
DENISOV S P *et al* 1971 *Phys. Lett.* **36B** 415
DOLEN R, HORN D and SCHMID C 1967 *Phys. Rev. Lett.* **19** 402
—— 1968 *Phys. Rev.* **166** 1768
EDEN R J 1967 *High Energy Collisions of Elementary Particles* (London: Cambridge University Press)
—— 1970 'Strong interactions of elementary particles' in *Essays in Physics* ed G K T Conn and G Fowler (London: Academic Press)
—— 1971 *Rev. Mod. Phys.* **43** 15
EDEN R J, LANDSHOFF P V, OLIVE D I and POLKINGHORNE J C 1966 *The Analytic S Matrix* (London: Cambridge University Press)
FEDERBUSH P G and GRISARU M 1963 *Ann. Phys.* **22** 263, 299
FEYNMAN R P 1969a *Phys. Rev. Lett.* **23** 1415
—— 1969b *High Energy Collisions* ed C N Yang (New York: Gordon and Breach) p237
FOLEY K J *et al* 1967 *Phys. Rev. Lett.* **19** 193, 330
FOX G C and QUIGG C 1970 *UCRL Rep.* 20001 (Berkeley, California: UCRL)
FRANCO V and GLAUBER R J 1966 *Phys. Rev.* **142** 1195
FRAUTSCHI S C and MARGOLIS B 1968 *Nuovo Cim.* **56A** 1155
FUBINI S 1963 *Strong Interactions and High Energy Physics* ed R G Moorhouse (Edinburgh: Oliver and Boyd)
GIACOMELLI G 1970 *Prog. Nucl. Phys.* **12** part 2
—— 1971 *Proc. Amsterdam Conf. on Elementary Particles* (Amsterdam: North Holland) to be published
GLAUBER R J 1955 *Phys. Rev.* **100** 242
GRIBOV V N 1962a *Sov. Phys.-JETP* **14** 1395
—— 1962b *Sov. Phys.-JETP* **15** 873
HAGEDORN R 1965 *Suppl. Nuovo Cim.* **3** 147
—— 1968 *Suppl. Nuovo Cim.* **6** 311
HAGEDORN R and RANFT J 1968 *Suppl. Nuovo Cim.* **6** 169
HEISENBERG W 1943 *Z. Phys.* **120** 513, 673
HONECKER R *et al* 1969 *Nucl. Phys.* B **13** 571
HORN D 1972 *Phys. Rep.* to be published
HYAMS B *et al* 1971 *Phys. Lett.* **35B** 610
IGI K 1962 *Phys. Rev. Lett.* **9** 76
—— 1963 *Phys. Rev.* **130** 820
IGI K and MATSUDA S 1967a, *Phys. Rev. Lett.* **18** 625
—— 1967b *Phys. Rev.* **163** 1622
JACKSON J D 1969 *Proc. Lund Int. Conf. on Elementary Particles* ed G von Daerdel (Stockholm: Swedish Institute of Physics)
JACOB M 1971 *Lecture Notes at Les Houches Summer School* (1971) to be published.
JONES L W *et al* 1970 *Phys. Rev. Lett.* **25** 1679
KALMUS G 1972 *Rep. Prog. Phys.* **35** to be published (London: Institute of Physics)
KANE G L *et al* 1969 *Phys. Rev.* **182** 1579
—— 1970 *Phys. Rev. Lett.* **25** 1519
KIBBLE T W B 1963 *Phys. Rev.* **131** 2282
KOBA S and NIELSON H B 1969 *Nucl. Phys.* B **10** 633
LANDSHOFF P V and POLKINGHORNE J C 1969 *Phys. Rev.* **181** 1989
LINDENBAUM S 1969 *Pion–Nucleon Scattering*, ed G Shaw and D Wong (New York: Wiley)
LOGUNOV A A, SOLOVIEV L D and TAVKHELIDZE A N 1967 *Phys. Lett.* **24B** 181

LOHRMAN E 1969 *Proc. Lund Int. Conf. on Elementary Particles* ed G von Daerdel (Stockholm: Swedish Institute of Physics)
LOVELACE C 1968 *Phys. Lett.* **28B** 264
MANDELSTAM S 1958 *Phys. Rev.* **112** 1344
—— 1963 *Nuovo Cim.* **30** 1127, 1148
MARTIN A 1969 *Scattering Theory: Unitarity, Analyticity and Crossing* (Berlin: Springer-Verlag)
MARTIN A D and SPEARMAN D 1970 *Elementary Particle Theory* (Amsterdam: North-Holland)
PHILLIPS R J N 1971 *Proc. Amsterdam Conf. on Elementary Particles* (Amsterdam: North-Holland) to be published
PILKUHN H 1968 *The Interactions of Hadrons* (Amsterdam: North-Holland)
POLKINGHORNE J C 1963 *J. Math. Phys.* **4** 503, 1393, 1396
—— 1965 *Nuovo Cim.* **36** 857
POMERANCHUK I Ya 1956 *Sov. Phys.-JETP* **3** 306
—— 1958 *Sov. Phys.-JETP* **7** 499
REGGE T 1959 *Nuovo Cim.* **14** 951
—— 1960 *Nuovo Cim.* **18** 947
ROY S M 1972 *Phys. Rep.* to be published
SCHMID C 1968 *Phys. Rev. Lett.* **20** 689
SMITH D B *et al* 1970 *Phys. Rev. Lett.* **25** 1072
SONDEREGGER P *et al* 1966 *Phys. Lett.* **20** 75
TER MATIROSYAN K A 1963 *Sov. Phys.-JETP* **17** 233
—— 1966, Berkeley Conference Report, see Van Hove (1966).
VAN HOVE L 1966 International Conference on High Energy Physics, Berkeley ed M Alston-Garnjost (Berkeley: University of California Press)
—— 1969a *Phys. Lett.* **28B** 429
—— 1969b *Nucl. Phys.* B **9** 331
—— 1971 *Phys. Rep.* **1** No 7 347
VENEZIANO G 1968 *Nuovo Cim.* **57A** 190
VIRASORO M 1969a *Phys. Rev.* **184** 1621
—— 1969b *Phys. Rev. Lett.* **22** 37
WEST G B and YENNIE D R 1968 *Phys. Rev.* **172** 1413
ZACHARIASEN F 1971 *Phys. Rep.* **2**C 1
ZACHARIASEN F and ZWEIG G 1967 *Phys. Rev.* **160** 1322, 1326